The Electronic Structure of Cu_A: A Novel Mixed-Valence Dinuclear Copper Electron-Transfer Center

J. A. Farrar,[†] F. Neese,[‡] P. Lappalainen,[§] P. M. H. Kroneck,[‡] M. Saraste,[§] W. G. Zumft,[||] and A. J. Thomson*,[†]

Contribution from the School of Chemical Sciences, University of East Anglia, Norwich NR4 7TJ, U.K., Fakultät für Biologie, Universität Konstanz, D-78434 Konstanz, Germany, European Molecular Biology Laboratory, D-69012 Heidelberg, Germany, and Lehrstuhl für Mikrobiologie, Universität Fridericiana, D-76128 Karlsruhe, Germany

Received June 3, 1996[⊗]

Abstract: Cu_A, an electron transfer center present in cytochrome *c* oxidase, COX, and nitrous oxide reductase, N_2-OR, is a dimeric copper complex with four ligands, two cysteine thiols bridging the metal ions and two terminal histidine residues. The center cycles between the mixed-valence state [Cu(I),Cu(II)] and the reduced state [Cu(I),-Cu(I)]. The EPR, optical absorption, low-temperature magnetic circular dichroism, and CD spectra of three proteins containing the mixed-valence state of Cu_A have been measured between 33 000 and 5000 cm^{-1}. These results point to two forms of the chromophore, one in the enzyme N_2OR of *Pseudomonas stutzeri*, lacking its catalytic center, and also in a water soluble domain of subunit II of *Paracoccus denitrificans* COX and the other, referred to as Cu_A*, in a site engineered into a soluble domain of subunit II of the quinol oxidase in *Escherichia coli*. An assignment of the electronic spectrum has been made in terms of a covalent planar core $[Cu_2(SR)_2]^+$ with a Cu−S distance of 2.2 Å, a Cu−Cu distance of 2.5 Å, and a Cu−S−Cu angle of 70°. Molecular orbitals arising from five 3d orbitals on each copper and two lone-pair thiolate orbitals on each cysteine ligand divide into three sets, four bonding (with respect to the Cu−S interaction) orbitals at lower energy, four antibonding orbitals at higher energy, and six intermediate nonbonding orbitals. The inversion center of the copper core imposes rather strict selection rules giving rise to two pairs of allowed electronic transitions, polarized along either the S−S or the Cu−Cu axis. A delocalization energy of ∼4500 cm^{-1} can be estimated from the data, which is at least 1 order of magnitude larger than the vibrational energies of the core, accounting for the stability of the class III or delocalized mixed-valence form. The Cu_A sites in COX and N_2OR have essentially identical electronic structures with complete delocalization. However, the Cu_A* site shows partial trapping of the valences. The close approach, to ∼2.3 Å, of the backbone carbonyl group of a conserved glutamic acid residue is proposed to be responsible for this partial localization. Cu_A is a highly covalent planar rhomb which provides an effective path, with low reorganization energy, for electron transfer across subunit II from cytochrome *c* to the cytochromes *a* and possibly a_3 of COX.

Introduction

Cytochrome *c* oxidase (COX) and nitrous oxide reductase (N_2OR) possess a novel electron storage and transfer center called Cu_A. In the case of COX this center receives electrons from soluble cytochrome *c* and transfers them to cytochrome *a*, whereas in N_2OR, Cu_A is believed to transfer electrons between a cytochrome *c* and the catalytically active site at which N_2O is reduced. A wealth of spectroscopic evidence dating back to 1962 has shown that Cu_A has a structure different from that of the blue or type I copper electron-transfer centers exemplified by azurin and plastocyanin.[1−12] The X-band electron paramagnetic resonance (EPR) spectrum of Cu_A in COX, first recorded by Beinert et al.,[1] is a broad quasi-axial signal lacking well-resolved copper hyperfine coupling. This led to the first suggestion that Cu_A may be a dinuclear copper center. The small copper hyperfine coupling constant was explained by the presence of a cysteine ligand with high copper−thiolate covalence placing the unpaired electron largely on the ligand and thus reducing coupling to the copper nucleus.[13]

In COX the optical properties of Cu_A are obscured in part by intense and overlapping transitions from the two cyto-

* Author to whom correspondence should be addressed. Telephone/FAX: (+44) 1603 592710. E-mail: a.thomson@uea.ac.uk.
[†] University of East Anglia.
[‡] Universität Konstanz.
[§] European Molecular Biology Laboratory.
[||] Universität Fridericiana.
[⊗] Abstract published in *Advance ACS Abstracts,* October 15, 1996.

(1) Beinert, H.; Griffiths, D. E.; Wharton, D. C.; Sands, R. H. *J. Biol. Chem.* **1962**, *237*, 2337−2346.
(2) Mims, W. B.; Peisach, J.; Shaw, R. W.; Beinert, H. E. *J. Biol. Chem.* **1980**, *255*, 6843−6846.
(3) Greenwood, C.; Hill, B. C.; Barber, D.; Eglinton, D. G.; Thomson, A. J. *Biochem. J.* **1983**, *215*, 303−316.
(4) Scott, R. A.; Zumft, W. G.; Coyle, C. L.; Dooley, D. M. *Proc. Natl. Acad. Sci. U.S.A.* **1989**, *86*, 4082−4086.
(5) Gurbiel, R. J.; Fann, Y.-C.; Surerus, K. K.; Werst, M. M.; Musser, S. M.; Doan, P. E.; Chan, S. I.; Fee, J. A.; Hoffman, B. M. *J. Am. Chem. Soc.* **1993**, *115*, 10888−10894.
(6) Blumberg, W. E.; Peisach, J. *Biochim. Biophys. Acta* **1966**, *126*, 269−273.
(7) Dooley, D. M.; McGuirl, M. A.; Rosenzweig, A. C.; Landin, J. A.; Scott, R. A.; Zumft, W. G.; Devlin, F.; Stephens, P. J. *Inorg. Chem.* **1991**, *30*, 3006−3011.
(8) Gewirth, A. A.; Solomon, E. I. *J. Am. Chem. Soc.* **1988**, *110*, 3811−3819.
(9) Peisach, J.; Levine, W. G.; Blumberg, W. E. *J. Biol. Chem.* **1967**, *242*, 2847−2855.
(10) Tullius, T.; Frank, P.; Hodgson, K. O. *Proc. Natl. Acad. Sci. U.S.A.* **1978**, *75*, 4069−4073.
(11) Roberts, J. E.; Cline, J. F.; Lum, V.; Freeman, H.; Gray, H. B.; Peisach, J.; Reinhammer, B.; Hoffman, B. M. *J. Am. Chem. Soc.* **1984**, *106*, 5324−5330.
(12) Coremans, J. W. A.; van Gastel, M.; Poluektov, O. G.; Groenen, E. J. J.; den Blaauwen, T.; van Pouderoyen, G.; Canters, G. W.; Nar, H.; Hammann, C.; Messerschmidt, A. *Chem. Phys. Lett.* **1995**, *235*, 202−210.
(13) Peisach, J.; Blumberg, W. E. *Arch. Biochem. Biophys.* **1974**, *165*, 691−708.

S0002-7863(96)01871-9 CCC: $12.00

chromes *a* and a_3. The only absorption band which could be assigned to Cu_A was a peak at ~830 nm. However, low-temperature magnetic circular dichroism (MCD) magnetization characteristics were used to deconvolute the contribution of low-spin heme from that of Cu_A.[3] The application of a novel optical-microwave double-resonance method confirmed the presence of optical transitions of Cu_A at ~480 and 520 nm, lying below the heme absorption MCD.[14] The similarity between the Cu_A centers in COX and N_2OR was first shown by a comparison of the room-temperature MCD spectrum of N_2OR and the low-temperature MCD spectrum of Cu_A.[7] This was subsequently confirmed by comparison with the MCD spectra of N_2OR determined at low temperature.[15] For many years models were based upon a mononuclear copper center although it was clear from EPR and MCD evidence that the center must possess more than one thiolate ligand and was electronically quite distinct from any of the structurally characterized type 1 copper sites. However, a bisthiolate mononuclear copper center, as observed in, for example, copper substituted into the catalytic site of horse liver alcohol dehydrogenase, did not produce the very intense bisignate MCD bands at 480 and 520 nm.[16] The possibility that Cu_A is a dinuclear copper center was raised anew when Kroneck and colleagues showed that N_2OR contains, in the oxidized resting state, a Cu_A-like center having an EPR spectrum similar to that of COX but with some resolved copper hyperfine coupling at $g_{||}$.[17,18] The form of this hyperfine coupling has been analyzed in detail at several microwave frequencies[19−22] and has been shown to be characteristic of a single unpaired electron interacting with two equivalent copper nuclei. This indicated that Cu_A is a mixed-valence (MV) class IIIA dimer[23] in which both copper ions must be equivalent.

As a result of extensive sequencing of the genes of COX from many sources, it became clear that Cu_A lies in subunit II.[24] Furthermore, sequence analysis showed that this subunit contains a pair of membrane-anchor helices plus a domain with striking similarities to the cupredoxin fold of blue copper proteins.[25] A detailed sequence comparison revealed a clear similarity in the primary structure between the Cu_A-binding domains of N_2OR and subunit II of COX.[26] These results enabled a putative copper-binding consensus sequence to be proposed in which the relationship between the blue copper center and Cu_A emerged; see Scheme 1.

The common ligands of the single copper site in blue copper proteins are two histidine and one cysteine residues with, in most cases, a weak further interaction between the metal ion and methionine with a long copper−sulfur interaction at ~2.8 Å.[31] The Cu_A-binding motif contains additional residues, including an invariant cysteine residue, lying between the cysteine and the adjacent residue of the blue copper consensus sequence, Scheme 1, to generate a consensus binding sequence of $H-(X)_{34}-C-(X)_3-C-(X)_3-H-(X)_2-M$ for Cu_A.[24,26]

Scheme 1

P. stutzeri N_2OR[26]	**H583**	-34-	**C618**	S	W	F	**C622**	H	A	L	**H626**	M	E	**M629**
Mitochondrial COX[24,27]	**H161**	-34-	**C196**	S	E	I	**C200**	G	S	N	**H204**	S	F	**M207**
P. denitrificans SUII[24]	**H181**	-34-	**C216**	S	E	L	**C220**	G	I	N	**H224**	A	Y	**M227**
E.coli QOX CyoA[24,28]	N	-34-	S	A	S	Y	S	G	P	G	F	S	G	**M218**
E. coli Purple CyoA[29]	**H172**	-34-	**C207**	A	E	I	**C211**	G	P	G	**H215**	S	G	**M218**
T. versutus Amicyanin[30]	**H54**	-38-	**C93**	-	-	-	-	-	T	P	**H96**	P	F	**M99**
Amicyanin 'Cu_A'[30]	**H54**	-38-	**C93**	A	E	I	**C97**	G	P	G	**H101**	S	G	**M104**

A variety of water soluble proteins containing only a single Cu_A center are now available. The first example was N_2OR V, a form of nitrous oxide reductase prepared from a Tn5 insertion mutant of *Pseudomonas stutzeri* which lacks enzymatic activity but does contain Cu_A.[17,32,33] A truncated form of subunit II of COX in which the transmembrane anchor helices are missing, but in which the Cu_A binding site is present, has been obtained by genetic manipulation for *Paracoccus denitrificans*,[34] *Bacillus subtilis*,[35] and *Synechocystis* spp.[36] In addition a Cu_A binding site has been engineered into the blue copper proteins amicyanin from *Thiobacillus versutus*[30] and azurin from *Pseudomonas aeruginosa*.[37] Finally a Cu_A binding site has been engineered into the soluble domain of subunit II from the quinol oxidase (QOX) of *Escherichia coli*, see Scheme 1 for details of the mutagenesis, to generate the purple CyoA protein.[38,39] For brevity and clarity this engineered Cu_A center will be referred to as Cu_A* throughout the remainder of this paper.

The availability of considerable quantities of engineered water soluble protein containing the Cu_A site has led rapidly to clarification of the structure of the Cu_A center. A set of studies of site-directed mutant forms of PdII (the soluble domain of subunit II of *P. denitrificans* cytochrome *c* oxidase expressed in *E. coli*) and CyoA showed that all the residues of the consensus sequence H172, H215, C207, C211, and M218 are required for the binding of a pair of copper ions to give a form characteristic of Cu_A.[34,39] Electrospray mass spectrometry[34] showed that a pair of copper ions are bound to the soluble domain of PdII. The mass difference between the apo and holo forms of the protein implied that no exogenous ligands such as

(14) Thomson, A. J.; Greenwood, C.; Peterson, J.; Barrett, C. P. *J. Inorg. Biochem.* **1986**, *28*, 195−205.
(15) Farrar, J. A.; Thomson, A. J.; Cheesman, M. R.; Dooley, D. M.; Zumft, W. G. *FEBS Lett.* **1991**, *294*, 11−15.
(16) Farrar, J. A.; Formicka, G.; Zeppezauer, M.; Thomson, A. J. *Biochem. J.* **1996**, *317*, 447−456.
(17) Riester, J.; Zumft, W. G.; Kroneck, P. M. H. *Eur. J. Biochem.* **1989**, *178*, 751−762.
(18) Coyle, C. L.; Zumft, W. G.; Kroneck, P. M. H.; Körner, H.; Jakob, W. *Eur. J. Biochem.* **1985**, *153*, 459−467.
(19) Antholine, W. E.; Kastrau, D. H. W.; Steffens, G. C. M.; Buse, G.; Zumft, W. G.; Kroneck, P. M. H. *Eur. J. Biochem.* **1992**, *209*, 875−881.
(20) Neese, F.; Zumft, W. G.; Antholine, W. E.; Kroneck, P. M. H. *J. Am. Chem. Soc.* **1996**, *118*, 8692−8699.
(21) Kroneck, P. M. H.; Antholine, W. A.; Riester, J.; Zumft, W. G. *FEBS Lett.* **1988**, *242*, 70−74.
(22) Kroneck, P. M. H.; Antholine, W. E.; Kastrau, D. H. W.; Buse, G.; Steffens, G. C. M.; Zumft, W. G. *FEBS Lett.* **1990**, *268*, 274−276.
(23) Robin, M. B.; Day, P. *Adv. Inorg. Chem. Radiochem.* **1967**, *10*, 247−422.
(24) Saraste, M. *Q. Rev. Biophys.* **1990**, *23*, 331−366.
(25) Holm, L.; Saraste, M.; Wikström, M. *EMBO J.* **1987**, *6*, 2819−2823.
(26) Zumft, W. G.; Dreusch, A.; Löchelt, S.; Cuypers, H.; Friedrich, B.; Schneider, B. *Eur. J. Biochem.* **1992**, *208*, 31−40.
(27) Anderson, S.; de Bruijn, M. H. L.; Coulson, A. R.; Eperon, I. C.; Sanger, F.; Young, I. G. *J. Mol. Biol.* **1982**, *156*, 683−717.
(28) Chepuri, V.; Lemieux, L.; Au, D. C.-T.; Gennis, R. B. *J. Biol. Chem.* **1990**, *265*, 11185−11192.
(29) Wilmanns, M.; Lappalainen, P.; Kelly, M.; Sauer-Eriksson, E.; Saraste, M. *Proc. Natl. Acad. Sci. U.S.A.* **1995**, *92*, 11955−11959.
(30) Dennison, C.; Vijgenboom, E.; de Vries, S.; van der Oost, J.; Canters, G. W. *FEBS Lett.* **1995**, *365*, 92−94.
(31) Adman, E. T. *Adv. Protein Chem.* **1991**, *42*, 145−197.
(32) Viebrock, A.; Zumft, W. G. *J. Bacteriol.* **1988**, *170*, 4658−4668.
(33) Zumft, W. G.; Dreusch, A. In *Nitrogen Fixation: Fundamentals and Applications*; Tikhonovich, I. A., Provorov, N. A., Romanov, V. I., Newton, W. E., Eds.; Kluwer: Dordrecht, The Netherlands, 1995.
(34) Lappalainen, P.; Aasa, R.; Malmström, B. G.; Saraste, M. *J. Biol. Chem.* **1993**, *268*, 26416−26421.
(35) von Wachenfeldt, C.; de Vries, S.; van der Oost, J. *FEBS Lett.* **1994**, *340*, 109−113.
(36) Lappalainen, P. *Biological Research Reports*; Univ. of Jyväskylä: Jyväskylä, 1995; Vol. 44.
(37) Hay, M.; Richards, J. H.; Lu, Y. *Proc. Natl. Acad. Sci. U.S.A.* **1996**, *93*, 461−464.
(38) van der Oost, J.; Lappalainen, P.; Musacchio, A.; Warne, A.; Lemieux, L.; Rumbley, J.; Gennis, R. B.; Aasa, R.; Pascher, T.; Malmström, B. G.; Saraste, M. *EMBO J.* **1992**, *11*, 3209−3217.
(39) Kelly, M.; Lappalainen, P.; Talbo, G.; Haltia, T.; van der Oost, J.; Saraste, M. *J. Biol. Chem.* **1993**, *268*, 16781−16787.

oxide, hydroxide, or sulfide were needed to generate a Cu_A center. These results, together with the evidence from EPR spectroscopy showing that both copper ions must have equivalent coordination sites, rather strictly constrained the number of possible structures for Cu_A. For a period of time both terminal and bridged thiolate ligation modes were considered by a number of different groups.

Within the last year three crystal structures of proteins containing Cu_A centers have been published, namely that of oxidized bovine heart COX at 2.8 Å,[40] of *P. denitrificans* COX also at 2.8 Å,[41] and finally of CyoA from *E. coli* at 2.3 Å with[29] and without[42] the Cu_A* center. All three structures show a dimeric copper site with four ligands, namely two cysteine thiolate groups bridging a pair of copper ions each of which is ligated by a terminal histidine residue. The resolution of the structure is not high in the case of the two COX structures. For the bovine heart COX the anomolous Fourier map showed a single metal site although the peak height was too high to be attributable to a single copper ion. The copper−copper distance of 2.8 Å must be regarded as preliminary given the resolution of the data. The structure of the Cu_A site in *P. denitrificans* COX was refined on the basis of a dinuclear copper site with two bridging thiolates and two terminal histidines. However, the metrical parameters can only be quoted approximately. The structure of purple CyoA, on the other hand, at considerably higher resolution was the first to establish unequivocally the bridged coordination mode. Figure 1a shows a schematic drawing of the dinuclear copper site in purple CyoA, Cu_A*, in which the metrical parameters of ref 29 are given. A projection of the structure almost along the S−S axis is given in Figure 1b. The four atoms, Cu_2S_2, form a rhomb which is planar to within 1.47°. The copper−copper distance is 2.48 ± 0.1 Å, the N−N axis of the pair of histidine ligands, H172 and H215, is tilted by 10−15° from the Cu−Cu direction. One copper atom sits 0.28 Å above while the other copper atom sits 1.01 Å below the ligand plane NS_2 defined by C207, C217, and either H172 or H215, respectively. A fourth atom lies almost perpendicular to this plane; for one copper ion the S^{δ} atom of M218 lies 3.02 Å from the copper and for the other metal ion the oxygen atom of the backbone carbonyl of E209 is 2.28 Å from the copper. This contrasts with the structural evidence from bovine heart and *P. denitrificans* COX, in which the S^{δ} atom of the conserved methionine residue and the carbonyl oxygen of the glutamic acid residue both lie ∼3.0 Å from the nearest copper ion.

The electronic structure of this novel MV dinuclear copper−thiolate center is of considerable interest. We have gathered a wide range of absorption, MCD, and CD (circular dichroism) spectra as well as EPR spectra for both Cu_A and Cu_A*, and we present here a comparison of these data together with a theoretical study of the electronic energy levels of this center. This has enabled us to propose an assignment of the electronic spectrum. We show that the electronic structures of the Cu_A and Cu_A* sites are different, and we identify the likely structural variation which gives rise to these differences.

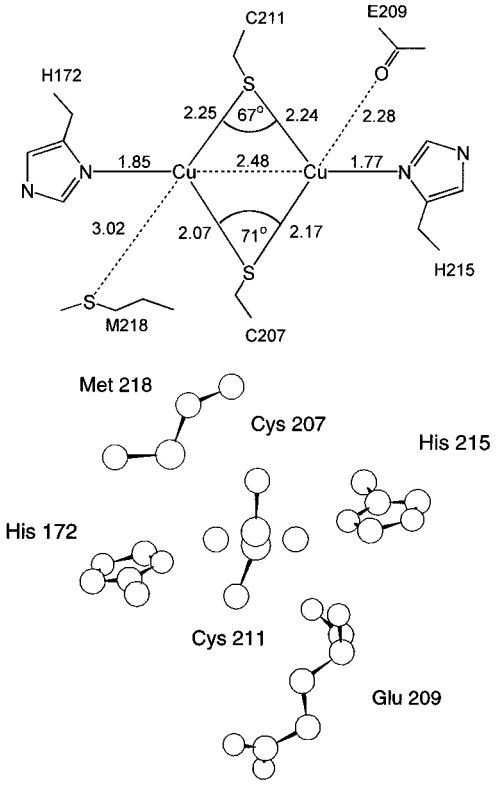

Figure 1. The structure of the Cu_A* site in *E. coli* QOX. (a) Schematic drawing looking along the *z*-axis onto the Cu_2S_2 rhomb and showing the metrical parameters. (b) View along the S−S axis (*y*-axis) showing the spatial orientation of the copper ligands. The atom positions and distances were taken from the X-ray crystallographic data of purple CyoA.[29]

Experimental Methods

A. Protein Purification. *P. denitrificans* Cu_A Domain Protein (PdII). The soluble Cu_A domain was expressed in *E. coli* BL21(DE3) cells as described previously.[34] Purification of the protein via inclusion bodies and reconstitution with copper was as described.[34,43]

For spectroscopic measurements the sample was exchanged on a Sephadex G-25 column (PD10, Pharmacia) into 50 mM HEPES (pH 6.0) and then concentrated at 5 °C in a Centricon 10 concentrator (Amicon). When required, glassing agent was added after exchange of buffer. Protein concentrations were determined using the millimolar extinction coefficient of 48.7 mM^{-1} cm^{-1} at 278 nm for the purified Cu_A domain protein. This value is based on a protein concentration determined by amino acid composition. The total copper content of the Cu_A domain was chemically measured by the biquinoline method.[44] The sample used in this study contained 1.8 Cu/protein. The purity of the Cu_A domain protein samples was determined by polyacrylamide gel electrophoresis in the presence of SDS using the buffer system of Laemmli,[45] which resulted in a single observable band.

***P. stutzeri* Nitrous Oxide Reductase (N_2OR V).** The mutant form of nitrous oxide reductase used in this study was obtained from strain MK402 of *P. stutzeri* ATCC 14405 which is defective in copper chromophore biosynthesis.[32,46] The bacterium was grown in wild type medium[18] supplemented with kanamycin and streptomycin. The nitrous oxide reductase was purified as for the wild type enzyme.[18]

Metal analysis of the purified protein was performed by atomic absorption spectroscopy using a Varian spectrophotometer with a carbon rod atomizer. Protein determination was by the method of Lowry.[47] The MK402 mutant nitrous oxide reductase used for this study contained 1.7 copper atoms per 140 kDa α2 dimer. No other metals were present. For spectroscopic measurements the buffer was

(40) Tsukihara, T.; Aoyama, H.; Yamashita, E.; Tomizaki, T.; Yamaguchi, H.; Shinzawa-Itoh, K.; Nakashima, R.; Yaono, R.; Yoshikawa, S. *Science* **1995**, *269*, 1069−1074.
(41) Iwata, S.; Ostermeier, C.; Ludwig, B.; Michel, H. *Nature* **1995**, *376*, 660−669.
(42) van der Oost, J.; Musacchio, A.; Pauptit, R. A.; Ceska, T. A.; Wierenga, R. K.; Saraste, M. *J. Mol. Biol.* **1993**, *229*, 794−796.
(43) Farrar, J. A.; Lappalainen, P.; Zumft, W. G.; Saraste, M.; Thomson, A. J. *Eur. J. Biochem.* **1995**, *232*, 294−303.
(44) Broman, L.; Malmström, B. G.; Aasa, R.; Vänngård, T. *J. Mol. Biol.* **1962**, *5*, 301−310.
(45) Laemmli, U. K. *Nature* **1970**, *227*, 680−685.
(46) Zumft, W. G.; Viebrock-Sambale, A.; Braun, C. *Eur. J. Biochem.* **1990**, *192*, 591−599.
(47) Lowry, O. H.; Rosebourgh, N. J.; Farr, A. L.; Randall, R. J. *J. Biol. Chem.* **1951**, *193*, 265−275.

50 mM Tris pH 7.5, with the addition of glassing agent to 50% by volume for low-temperature MCD measurements.

Enzymic activity was measured by the gas chromatography assay used for wild type nitrous oxide reductase as described in ref 18. The protein was inactive under this assay system. Attempts to incorporate additional copper were unsuccessful and did not result in observable N_2O reduction. In other preparations the level of copper present has ranged from 1.9 to 2.2 copper per dimer, although activity was never observed.[17] The level of copper in the mutant form is much reduced compared with the eight copper atoms per 140 kDa α2 dimer found for wild type *P. stutzeri* nitrous oxide reductase, which results in maximal observed activity.[17]

***E. coli* Quinol Oxidase Purple CyoA Protein.** Site-directed mutagenesis to introduce the Cu_A* center into the soluble domain of subunit II of *E. coli* quinol oxidase and subsequent protein purification has been described previously.[38,39] Metal analysis showed 1.7 mol of Cu/mol of protein.[39] For spectroscopic measurements the buffer was exchanged as for the PdII protein.

B. Spectroscopic Methods. Optical Spectroscopy. Absorption spectra were recorded using a Hitachi U4001 spectrophotometer with the sample at ambient temperature. Extinction coefficient values for the absorption spectra are quoted on a protein concentration basis.

MCD spectra were measured as previously described.[48] At low temperature the MCD spectrum is expected to be dominated by the C-term intensity and is thus dependent on the concentration of the paramagnetic chromophore.[49] Hence, the extinction coefficients quoted, $\Delta\epsilon = \epsilon_L - \epsilon_R$ (M^{-1} cm^{-1}), refer to the concentration of the paramagnetic copper chromophore present as determined by spin integration of the copper EPR signal and are not normalized for the magnetic field. Low-temperature optical spectroscopy requires the addition of a glassing agent, either glycerol or 1,2-ethandiol, to 50% by volume. The integrity of the protein samples in this solvent mix was monitored using both optical and EPR spectroscopies. Addition of cryoprotectant did not affect the spectroscopic properties of the proteins. Integration of the EPR signal before and after addition of glassing agent gave, within experimental error, the same percentage concentration of paramagnetic copper, showing the center to be unaffected by the solvent change. For optical spectroscopy in the near-infrared region of the spectrum, protein samples were exchanged into deuterated buffer.

CD spectra were recorded on samples at ambient temperature using the same spectrometers as for the MCD spectroscopy, namely a JASCO J500-D spectrometer for the wavelength region 300−1000 nm, and a laboratory-designed and -built spectrometer for the near-infrared region out to 2000 nm.[48] Extinction coefficients, $\Delta\epsilon = \epsilon_L - \epsilon_R$ (M^{-1} cm^{-1}), are quoted based on the protein concentration.

EPR Spectroscopy. EPR spectra were recorded on a Bruker ER-200D spectrometer equipped with an X-band cavity (9.4 GHz) and an Oxford Instruments ESR-900 helium flow cryostat. A modulation frequency of 100 kHz and a modulation amplitude of either 0.5 or 1 mT were used. To enable accurate simulation of the spectra and hence calculation of the *g*-values, the microwave frequency and magnetic field were measured by means of an external frequency counter and gaussmeter. Spectra were recorded under nonsaturating conditions to allow quantitative determination of the EPR detectable copper according to the method of Aasa and Vänngård[50] using a copper−EDTA standard; this typically involved a temperature of 20 K and a power of 200 nW.

C. Data Fitting and Simulation. To allow identification of the electronic transitions, the absorption, MCD, and CD spectra of all three proteins were fitted to a sum of Gaussian curves between 33 000 and 7500 cm^{-1}, using the curve fitting routine in the Origin software package (Microcal). As an aid to the assignment of the optical transitions, the ratio of the MCD C-term intensity to that of the optical absorption, $\bar{C}_0/\bar{D}_0$, has been calculated. The ratio of $\bar{C}_0$ and $\bar{D}_0$ for each band is easily calculated from the expressions in ref 49 once the experimental data have been fitted to Gaussian curves. Assuming that any MCD B-term intensity is negligible, as will be the case at 4.2 K, then for a given band

$$\frac{\bar{C}_0}{\bar{D}_0} = \frac{\Delta_{MCD}}{\Delta_{ABS}} \frac{\Delta\epsilon_{calc}}{\epsilon_{calc}} \frac{\nu_{ABS}}{\nu_{MCD}} \frac{kT}{\mu_B B}$$

where k is the Boltzmann constant, T is the absolute temperature, μ_B is the Bohr magneton, and B is the magnetic field strength at which the MCD spectrum is measured. The values of Δ, ν, $\Delta\epsilon_{calc}$, and ϵ_{calc} are those obtained from the Gaussian analysis. Thus 2Δ is the full width at half-maximum height (fwhm), ν_{ABS} and ν_{MCD} are the calculated energies of the band maxima for the absorbance and MCD spectra, respectively, ϵ_{calc} is the band height at ν_{abs} for the absorption spectrum, and $\Delta\epsilon_{calc}$ is the band height at ν_{MCD}. The value of $\Delta\epsilon_{calc}$ used in the above expression is increased by a factor of 1.25 compared to the value obtained from the Gaussian analysis to account for the nonlinearity of the MCD signal at 4.2 K and 5 T due to the onset of magnetization (saturation), as expected for a $S = {}^1/_2$ system, due to the Boltzman effect.

The oscillator strength, $f_{osc} = 4.3e^{-9} \times$ area of the curve, for each absorbance band and the Kuhn anisotropy factor $= \Delta\epsilon_{calc}/\epsilon_{calc}$, the ratio of the intensity of a transition in the CD spectrum to that in the absorbance spectrum,[51] have also been calculated.

The EPR spectra from PdII and purple CyoA have been simulated using the program EPR.[52] This program allows the simultaneous and independent variation of the **g**-tensor and any number of **A**-tensors as well as rotation of the **A**-tensor relative to the **g**-tensor.

D. Details of Semiempirical Calculations. Semiempirical INDO/S (intermediate neglect of differential overlap/spectroscopic parameterization) calculations[53,54] on a $[NH_3Cu(SCH_3)_2CuNH_3]^+$ model in C_i symmetry were similar to those described previously.[20,55] All state labels refer to the point group D_{2h} of the stripped NCuSSCuN unit. Reduction of β_d(Cu) to 20 eV is essential. The interaction factors $f_{p\pi p\pi} = f_{d\pi d\pi} = 0.585$ and $f_{p\sigma p\sigma} = f_{d\sigma d\sigma} = 1.266$ were used, and all other interaction factors were set to unity. The restricted open shell Hartree−Fock (ROHF) formalism of ref 55 was employed. We have shown[55] that spin polarization is of little importance in Cu_A, i.e. the ROHF solution is close to the spin-unrestricted Hartree−Fock solution and is therefore a suitable starting point for a configuration interaction with single excitations from the self-consistent field (SCF) state (CIS) treatment. All transitions into and from the singly occupied molecular orbital (SOMO) were included in the configuration interaction (CI). In addition, all configurations arising from excitation from the 13 highest doubly occupied into the five lowest unoccupied molecular orbitals (MOs) were included, leading to a total of 168 configurations. Inclusion of up to 288 configurations resulted in only minor changes to the calculated properties. With the present parameterization the ROHF-SCF-INDO/S method converged in typically 70−100 iterations to a $^2B_{2u}$ ground state, the next ground state, $^2B_{3u}$, being within 1000 cm^{-1}. For the calculation of spectra for the $^2B_{3u}$ ground state, these two low lying states were swapped after diagonalization of the CI matrix. Optical transition intensities were calculated in the dipole length formalism[56] including only one-center terms. The theoretical and computational methodology for calculating *g*-values and MCD C-term intensities will be fully described elsewhere. Essentially a number of states (typically around 50) belonging to the lowest energy CI roots were selected as a basis for the inclusion of spin−orbit coupling, again including only one-center terms. From the set of many electron states $\Psi_{0\alpha}...\Psi_{N\alpha}$ corrected with spin−orbit coupling, the theoretical C-term intensities and $\bar{C}_0/\bar{D}_0$ ratios were calculated according to Piepho and Schatz[49] where

(48) Thomson, A. J.; Cheesman, M. R.; George, S. J. *Methods Enzymol.* **1993**, *226*, 199−231.
(49) Piepho, S. B.; Schatz, P. N. *Group Theory in Spectroscopy with Applications to Magnetic Circular Dichroism*; Wiley-Interscience: New York, 1983.
(50) Aasa, R.; Vänngård, T. *J. Magn. Reson.* **1975**, *19*, 308−315.
(51) Kuhn, W. *Trans. Faraday Soc.* **1930**, *26*, 293−308.
(52) Neese, F. *QCPE* **1995**, *15*, 5.
(53) Zerner, M. C.; Loew, G. H.; Kirchner, R. F.; Mueller-Westerhoff, U. T. *J. Am. Chem. Soc.* **1980**, *102*, 589−599.
(54) Zerner, M. C. In *Reviews in Computational Chemistry*; Lipkowitz, K. B., Boyd, D. B., Eds.; VCH: Weinberg, Germany, 1990; pp 313−359.
(55) Kappl, R.; Neese, F.; Zumft, W. G.; Hüttermann, J.; Kroneck, P. M. H. Manuscript in preparation.
(56) Avery, J. B. *The Quantum Theory of Atoms, Molecules and Photons*; McGraw-Hill: London, 1972.

$$\bar{C}_0(\Psi_0 \rightarrow \Psi_J) = -\frac{i}{6}\sum_{\alpha\alpha'\lambda} \langle \Psi_{0\alpha'}|L+g_eS|\Psi_{0\alpha}\rangle[\langle \Psi_{0\alpha'}|m|\Psi_{J\lambda}\rangle\langle \Psi_{J\lambda}|m|\Psi_{0\alpha}\rangle] \quad (1)$$

$$\bar{D}_0(\Psi_0 \rightarrow \Psi_J) = {}^1/_6\sum_{\alpha\lambda} |\{\Psi_{0\alpha}|m|\Psi_{J\lambda}\rangle|^2$$

Here m is the electric dipole moment operator, and L and S are the operators for the total orbital and spin angular momentum, respectively. Simulated spectra were obtained by convoluting the theoretical spectra with a Gaussian line shape using a fwhm of 750 cm^{-1}. The structural parameters of the idealized model were as follows: Cu−S 2.22 Å, Cu−N 2.05 Å, Cu−S−Cu 71°, and a planar $Cu_2S_2N_2$ frame.

Experimental Results

A. EPR Spectra. The experimental EPR spectra of N_2OR V, PdII, and purple CyoA are presented in Figure 2, spectra A, B, and D, respectively. Integration of each of the signals yields the spin concentration. This value was found to be 50% ± 5% of the total copper content for all the proteins studied in this work, showing that the native state of both the Cu_A and Cu_A* centers is the MV [Cu(I),Cu(II)] state in which there is one unpaired electron resulting in an $S = {}^1/_2$ ground state.

The experimental spectra are axial with $g_{\|} > g_{\perp}$. The hyperfine splittings of $g_{\|}$ are extremely similar for N_2OR V and PdII (Figure 2, spectra A and B), with a seven-line splitting pattern clearly being observed for both proteins. Purple CyoA (Figure 2D), on the other hand, shows a more complex splitting pattern. In order to evaluate these differences, the spectra of a typical Cu_A center in PdII and the Cu_A* center in purple CyoA were simulated. The resulting spectra are presented in Figure 2, spectra C and E, respectively. For PdII $g_{max} = 2.19$, $g_{mid} = 2.03$, and $g_{min} = 1.99$. The hyperfine splitting pattern on g_{max} has been simulated with $A = 3.1$ mT for both copper nuclei, resulting in the now classic seven-line splitting pattern with an intensity ratio of 1:2:3:4:3:2:1.[18,19] Thus the Cu_A center is more accurately described as an average valence [Cu(1.5),Cu(1.5)] dimer than a mixed-valence [Cu(I),Cu(II)] dimer. A hyperfine splitting of 3.1 mT is extremely small for copper proteins, smaller even than that obtained for the blue copper proteins such as azurin (typically 7−8 mT[6]), and indicates a high degree of delocalization of the electron onto the copper ligands.[57] For purple CyoA the g-values obtained from simulation of the spectrum are $g_{max} = 2.20$, $g_{mid} = 2.02$, and $g_{min} = 2.00$. The g_{max} signal shows a more complex hyperfine splitting pattern than that observed in the PdII spectrum. It has been simulated with two slightly inequivalent copper nuclei with $A(1) = 6.8$ mT and $A(2) = 5.3$ mT. Thus the two copper nuclei are not in equivalent environments, and the degree of delocalization of the electron onto the ligands is less pronounced for Cu_A* than for the Cu_A centers studied here and elsewhere.[15,17,19,35,43]

B. Optical Spectra. The room-temperature absorption spectra, 4.2 K MCD spectra, and room-temperature CD spectra for N_2OR V, PdII, and purple CyoA from 33 000 to 7500 cm^{-1} are presented in Figures 3−5. No electronic transitions have been detected by low-temperature MCD between 5000 and 7500 cm^{-1}. In order to able to assign them, all the spectra in Figures 3−5 have been subjected to Gaussian deconvolution. The absorption, MCD, and CD spectra were first independently fitted to the minimum number of Gaussian curves, keeping the fwhm to a minimum. Then the absorbance and MCD spectra for each sample were iteratively refined until the energies and fwhm for a particular band were matched as closely as possible. Throughout the fitting procedure bands from both PdII and N_2OR V were required to remain close in energy, but the bands from purple CyoA were not restrained. A maximum of 11 different bands were identified in the region 33 000 to 7500 cm^{-1}. The results of the Gaussian analysis are presented in Tables 1 and 2 for PdII and purple CyoA, respectively. Deconvolution of the N_2OR V gave data identical to that of PdII, and hence they are not presented here. Simulated spectra, obtained as a sum of the individual Gaussian curves, are shown plotted

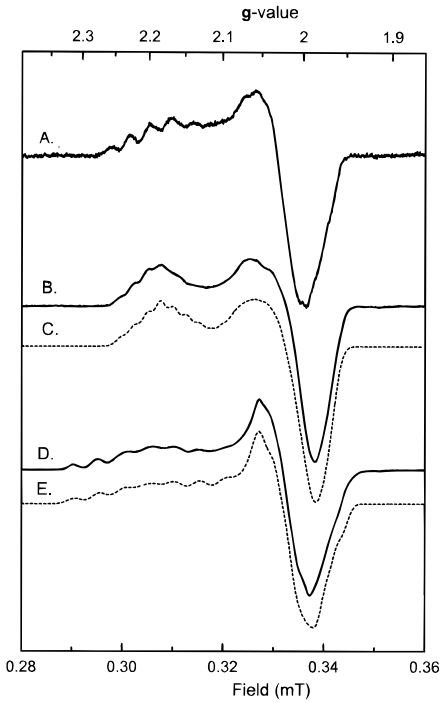

Figure 2. (A) EPR spectrum of N_2OR V. (B) EPR spectrum of PdII. (C) Simulated spectrum of PdII. (D) EPR spectrum of purple CyoA. (E) Simulated spectrum of purple CyoA. Measurement conditions for experimental spectra: 30 K, 200 nW power, 0.1 mT modulation.

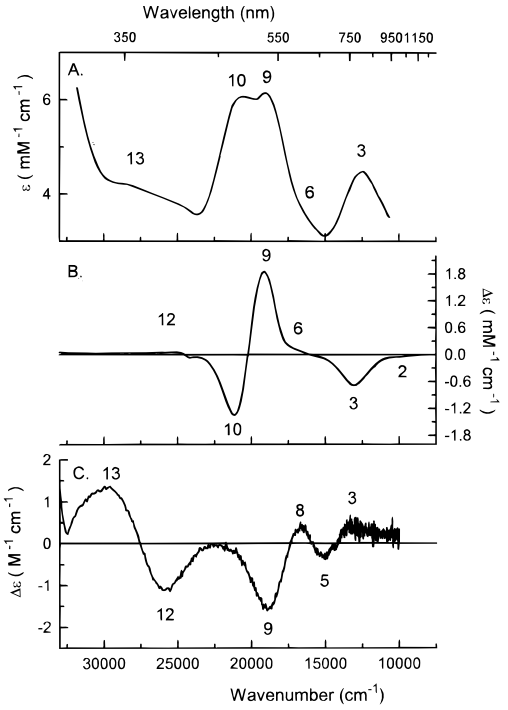

Figure 3. Optical data of N_2OR V from 33 000 cm^{-1} to 7500 cm^{-1}. (A) RT absorbance spectrum. (B) 4.2 K MCD spectrum. (C) RT CD spectrum.

(57) Shadle, S. E.; Penner-Hahn, J. E.; Schugar, H. J.; Hedman, B.; Hodgson, K. O.; Solomon, E. I. *J. Am. Chem. Soc.* **1993**, *115*, 767−776.

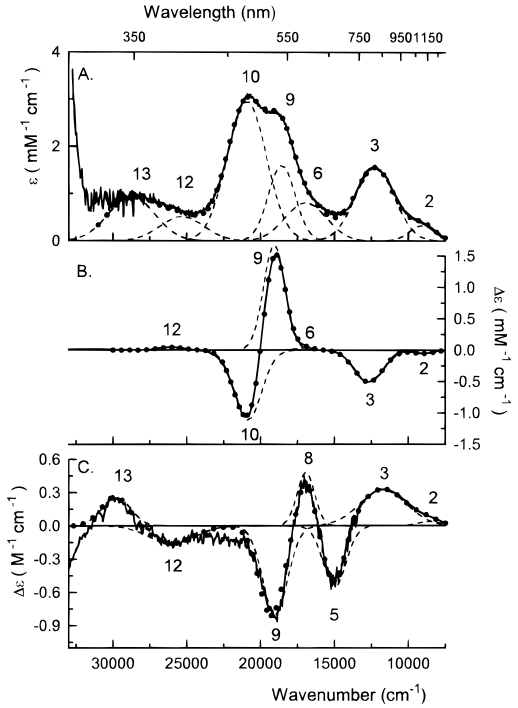

Figure 4. Optical data of PdII from 33 000 to 7500 cm^{-1}. (A) RT absorbance spectrum. (B) 4.2 K MCD spectrum. (C) RT CD spectrum.

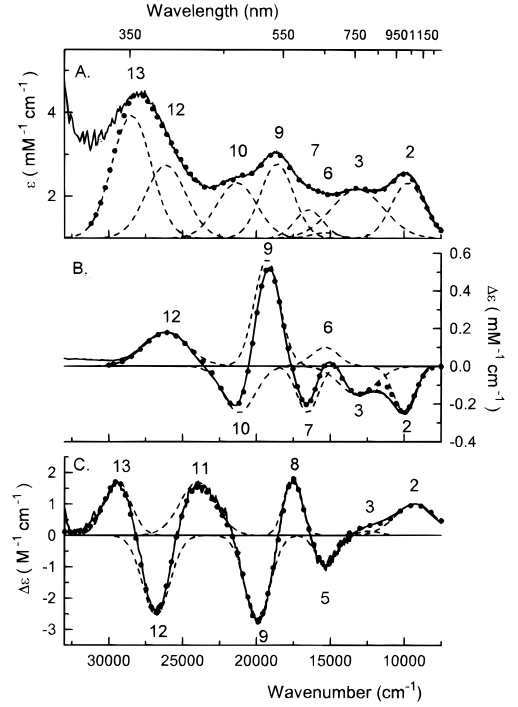

Figure 5. Optical data of purple CyoA from 33 000 to 7500 cm^{-1}. (A) RT absorbance spectrum. (B) 4.2 K MCD spectrum. (C) RT CD spectrum.

over the absorbance, MCD, and CD spectra of PdII and purple CyoA in Figures 4 and 5, together with the individual Gaussian curves.

The data in Figures 3 and 4 are strikingly similar. The MCD spectra are dominated by intense oppositely signed bands, labeled 9 and 10, and a negatively signed band, labeled 3. These spectra are in good agreement with those obtained originally from bovine heart COX.[3,14,58] Remarkably, the CD spectra of

(58) Greenwood, C.; Thomson, A. J.; Barrett, C. P.; Peterson, J.; George, G. N.; Fee, J. A.; Reichardt, J. *Ann. N.Y. Acad. Sci.* **1988**, *550*, 47−52.

Table 1. Detailed Analysis of the Optical Transitions for the Cu_A Center in PdII following Gaussian Deconvolution of the Experimental Data[a]

band	exptl energy (cm^{-1})	FWHM	oscillator strength	exptl C_0/D_0	Kuhn anisotropy factor
2	Abs: 9040	2056	0.0031		
	MCD: 9030	1762		−0.183	
	CD: 8610	1861			1.21×10^{-4}
3	Abs: 12 280	3106	0.0224		
	MCD: 12 690	2281		−0.334	
	CD: 11 720	3753			2.10×10^{-4}
5	CD: 15 000	1810			
6	Abs: 16 950	3313	0.0124		
	MCD: 17 000	1428		0.033	
8	CD: 16 955	1400			
9	Abs: 18 580	2146	0.0159		
	MCD: 19 080	1720		1.774	
	CD: 19 030	1982			4.94×10^{-4}
10	Abs: 20 940	3133	0.0427		
	MCD: 20 870	2155		−0.383	
12	Abs: 25 330	3500	0.0084		
	MCD: 26 055	2035		0.075	
	CD: 26 040	3540			3.10×10^{-4}
13	Abs: 28 155	4155	0.0152		
	CD: 29 800	2318			1.66×10^{-4}

[a] For details of the calculations, see the Experimental Methods section.

Table 2. Detailed Analysis of the Optical Transitions for the Cu_A* Center in Purple CyoA following Gaussian Deconvolution of the Experimental Data[a]

band	exptl energy (cm^{-1})	fwhm	oscillator strength	exptl C_0/D_0	Kuhn anisotropy factor
2	Abs: 9740	2654	0.0162		
	MCD: 10 000	1711		−0.1651	
	CD: 9280	3164			7.64×10^{-4}
3	ABS: 13 150	4193	0.0227		
	MCD: 13 145	2897		−0.1294	
	CD: 12 370	1674			1.16×10^{-4}
5	CD: 15 300	1575			
6	Abs: 15 350	2121	0.0001		
	MCD: 15 350	2121		0.9928	
7	Abs: 16 450	2272	0.0071		
	MCD: 116 530	1683		−0.3850	
8	CD: 17 555	1400			
9	Abs: 18 600	2631	0.0215		
	MCD: 19 280	2030		0.3460	
	CD: 19 930	1982			1.53×10^{-3}
10	Abs: 21 330	3198	0.0195		
	MCD: 21 170	2491		−0.2118	
11	Abs: 23 980	2867	0.0082		
	CD: 23 980	2867			3.25×10^{-3}
12	Abs: 26 130	3215	0.0258		
	MCD: 26 130	3518		0.1627	
	CD: 26 790	2161			1.46×10^{-3}
13	Abs: 28 450	3133	0.0422		
	CD: 29 400	2105			5.98×10^{-4}

[a] For details of the calculations, see the Experimental Methods section.

the Cu_A center in these two proteins are also extremely similar. The same number of bands with identical signs is found. Features of note are the oppositely signed CD bands, labeled 5 and 8, which lie at energies where there is little intensity in the absorption or the MCD spectra. In the region of the intense absorption and MCD bands, 9 and 10, there is only one CD active transition. Figures 3 and 4 show that the Cu_A sites in PdII and in N_2OR V are virtually identical in electronic structure. Hence, the coordination geometry of the ligands which dictates this structure must be the same. The CD spectra also reflect this similarity in spite of the low degree of sequence conservation, apart from the metal ligands around the Cu_A sites, in the two proteins.

By contrast, comparison of these two sets of data with those from the Cu_A* center in purple CyoA shows very substantial differences. The positions of the major bands in the absorption spectrum, 2, 3, 9, 10, and 13 in Figure 5A, are comparable to those from the Cu_A centers, Figures 3A and 4A. However, the overall intensity has decreased, and there are different intensity ratios for the bands in the Cu_A* spectrum, most noticably the increased intensity of band 13 compared with that for the Cu_A centers. The MCD spectrum of the Cu_A* center has also weakened in overall intensity, and there is a more even intensity distribution compared with those for the Cu_A. For example, the major feature around 19 000 cm^{-1}, band 9, is reduced in intensity from $\Delta\epsilon_{obs} = 1200\ M^{-1}\ cm^{-1}$ in the spectrum of PdII to $\Delta\epsilon_{obs} = 700\ M^{-1}\ cm^{-1}$ in the spectrum of purple CyoA, and band 2, at around 10 000 cm^{-1}, is substantially increased in the spectrum of Cu_A*. Despite the apparently different MCD spectra, Gaussian analysis has shown that the only difference is an additional band, band 7 in Figure 5B, present in the MCD spectrum of Cu_A*. The CD spectrum of Cu_A* has gained one additional band, band 11, compared with those obtained for the Cu_A centers. Taken together, the spectroscopic data show that it is likely that the Cu_A* center created in the soluble domain of subunit II from *E. coli* QOX is a close, although not exact, replica of the "true" Cu_A center present in COX and N_2OR V. Therefore, the structure obtained from the X-ray crystallography of Cu_A* is used as a starting point for the analysis of both types of center.

It is interesting to compare the optical data presented here with the data recently obtained from the soluble Cu_A domain from *Thermus thermophilus* COX.[59] The CD spectrum of *T. thermophilus* Cu_A domain protein has positive intensity between 400 and 500 nm, in contrast to the CD spectra from PdII and N_2OR V, but more like the CD spectrum of the Cu_A* center. Additionally, the absorbance spectrum of the Cu_A center in *T. thermophilus* shows increased intensity in the 360 nm band, comparable to the spectrum obtained from the soluble domain of *Synochocystis* spp. COX where the magneto-optical data can be interpreted in terms of slight differences between the coordination geometries of the two copper ions.[60] It is most likely that there is a virtually continuous variation in the degree of equivalence of the two copper ions in the dimeric Cu_A center from different sources. Thus, the Cu_A center in PdII and N_2-OR V has equivalent copper ions and is a true average-valence site, whereas for the Cu_A center in *T. thermophilus* and *Synochocystis* spp., the degree of delocalization is still high, although the two metal ions are slightly inequivalent. In the Cu_A* center the two copper ions are markedly inequivalent. The optical, CD, MCD, and EPR spectra are clearly highly sensitive reporters of this variation.

C. Orientation of the Cu_A g-Tensor and Polarization of the Optical Transitions. There is a considerable body of spectroscopic evidence obtained from oriented multilayers of bovine heart COX, originating from the work of Blasie and co-workers[61] who showed that highly oriented multilayers of COX could be deposited on substrates such as silica or mica. Studies have been reported with linearly polarized light,[61] with EPR spectroscopy,[62] with MCD spectroscopy,[58] and with EXAFS.[63] The crystal structure of bovine COX now enables deductions to be made about the orientations of the **g**-tensor and the polarizations of the optical transitions relative to the molecular framework for the chromophores in COX. Such data are an important aid in limiting the assignment choices.

The crystal structures of bovine heart and *P. denitrificans* COX show that the Cu−Cu axis of Cu_A lies approximately perpendicular to the membrane plane.[40,41] The S−S axis lies parallel to the membrane plane. The angle of the Cu−Cu axis with respect to the membrane normal cannot presently be deduced with high accuracy given the relatively low resolution of the X-ray structures. However, copper EXAFS of oriented membranes of COX provides further useful information. George et al.[63] identified a scattering due to an interaction, Cu−X, at approximately 2.6 Å. Although X was assigned to a sulfur atom, it is now clear from subsequent work[64] on a soluble Cu_A domain from *B. subtilis* that this scattering is due to the Cu−Cu interaction at approximately 2.5 Å. The EXAFS results on oriented membranes of COX[63] showed that this scattering peak was highly anisotropic, being almost zero when the X-ray electric vector was polarized in the membrane plane, but having a maximum value when the vector was at ±15° to the membrane normal. No data were reported at 0° to the normal. Hence, these data are consistent with a Cu−Cu axis lying within a cone with an axis normal to the membrane plane and a half angle of 15 °.

EPR spectra at Q-band of oriented bovine heart COX membranes[62] established the orientation of the Cu_A **g**-tensor, in which g_{max} lies at an angle of 63° to the membrane normal and g_{min} lies in the membrane plane. This shows that g_{max} lies approximately perpendicular to the Cu_2S_2 plane, that g_{min} lies along the S−S axis, and g_{mid} lies along the Cu−Cu direction, consistent with the theoretical analysis presented in ref 20.

MCD spectra of oriented membranes of COX,[58] with the circularly polarized light beam propagating along the membrane normal, showed no heme optical transitions. Because the heme rings are viewed edge-on, the heme optical transitions appear as one-dimensional or linearly polarized oscillators. Two orthogonal components of intensity are required for significant MCD intensity. However, the MCD spectra did reveal optical transitions arising from Cu_A, including the bands at 475, 525, and 708 nm. A comparison of the intensity ratios of these bands with the ratios obtained from an isotropic frozen glass of Cu_A domain shows that the band at 475 nm is relatively weaker, compared to the bands at 540 and 708 nm, in the spectrum obtained from the oriented membranes; hence this band is polarized along the Cu−Cu axis.

Results from MCD-detected microwave resonance at Q-band gave similar band shapes for Cu_A in COX with optical detection at 475, 520, and 800 nm[14] and for N_2OR V using detection at 475, 530, and 810 nm,[65] consistent with each transition having components polarized orthogonal to one another and to the direction of the g_z axis.

In summary, these results allow us to conclude that the **g**-tensor component g_{zz} lies approximately perpendicular to the plane of the Cu_2S_2 rhomb and that all the optical transitions are polarized in this plane, with bands being polarized either along the Cu···Cu or S···S direction. It is likely that the axes of both the **g**-tensor and the optical polarization tensor are tilted relative to the plane of the Cu_2S_2 rhomb, possibly by as much as 10−20°, since they are not required by symmetry to be collinear when the nitrogen ligands and the β-carbon atoms of

(59) Slutter, C. E.; Sanders, D.; Wittung, P.; Malmström, B. G.; Aasa, R.; Richards, J. H.; Gray, H. B.; Fee, J. A. *Biochemistry* **1996**, *35*, 3387−3395.

(60) Farrar, J. A.; Lappalainen, P.; Saraste, M.; Thomson, A. J. Unpublished data.

(61) Blasie, J. K.; Erecinska, M.; Samuels, S.; Leigh, J. S. *Biochim. Biophys. Acta* **1978**, *501*, 33−52.

(62) George, G. N. Personal communication.

(63) George, G. N.; Cramer, S. P.; Frey, T. G.; Prince, R. G. *Biochim. Biophys. Acta* **1993**, *1142*, 204−252.

(64) Blackburn, N. J.; Barr, M. E.; Woodruff, W. H.; van der Oost, J.; de Vries, S. *Biochemistry* **1994**, *33*, 10401−10407.

(65) Bingham, S. J. Ph.D. Thesis, University of East Anglia, Norwich, U.K., 1993.

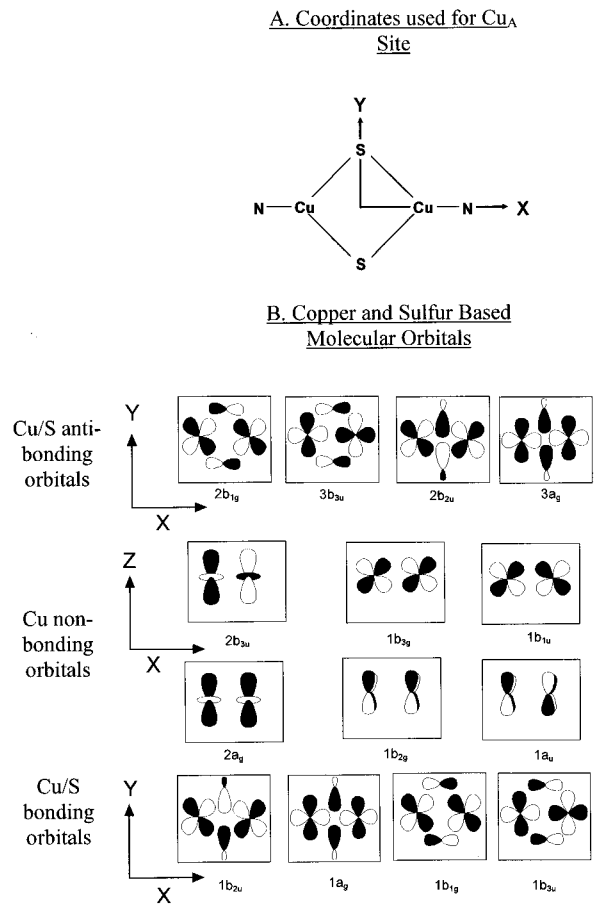

Figure 6. (A) Idealized D_{2h} Cu_A center showing the axis system used for interpretation of the optical spectra. (B) Schematic representation of the 14 copper−sulfur-based molecular orbitals required for assignment of the optical data. The MOs are labeled according to their one-electron orbital designation.

the thiolate ligands are taken into account. A more precise determination will only come from carrying out polarized optical and EPR spectroscopies on oriented single crystals of Cu_A centers.

Theoretical Model

A. Choice of Orbitals. The EPR properties of Cu_A, Figure 2 and discussed at length elsewhere,[20] show unequivocally that the electron spin is distributed equally over both halves of the MV dimer from 2 K to at least 100 K, suggesting that there is an element of symmetry relating the two halves. Cu_A therefore belongs to the "class III" MV dimers according to the classification of Robin and Day.[23] In this limiting case the SCF-MO method is expected to provide a good description of the electronic structure of MV dimers.[66] Properly constructed MOs must be either symmetric or antisymmetric with respect to this symmetry element. The X-ray structure of Cu_A* may be considered to show a center of inversion if only the first coordination sphere is considered. The coordinate system given in Figure 6 is used throughout. The idealized Cu_A center presented in Figure 6A belongs to the point group D_{2h}. When the protein surroundings are taken into account, the symmetry of the Cu_A center is undoubtly lower than this. However, the electronic structure apparently has a high effective symmetry. Therefore the D_{2h} group has been used throughout for the interpretation of data for the Cu_A center, and all relevent MOs have been designated according to the irreducible representations of the D_{2h} point group. The X-ray structure of Cu_A* shows that the histidine residues lie on a plane which is rotated by 15° relative to the Cu_2S_2 plane. This reduces the symmetry such that the highest possible point group would be C_{2h}. The effect of this reduction in symmetry to C_{2h} will be discussed in relation to the interpretation of the Cu_A* spectroscopic data.

The highest filled orbitals of the free thiolate ligand are formed from a doubly degenerate set of essentially sulfur p-orbitals which are perpendicular to the S−C bond direction,[67] while a C−S σ-bonding orbital lies 3−4 eV to lower binding energy. In an extensive series of studies, the bonding of these orbitals to the cupric ion in blue proteins has been clarified by Solomon and co-workers.[8,68−73] As shown by the work of this group, the doubly degenerate set splits into a pseudo-σ- and a π-orbital with respect to the copper−sulfur bond direction. In the optical spectrum of blue proteins, the transitions from the pseudo-σ- and the π-orbital to the SOMO are both observed in the visible region, while the transition from the low lying σ-orbital is predicted to occur in the far UV region.[8] A similar situation exists for the Cu_A center. As shown by the INDO/S calculations, one of the lone pairs of each thiolate ligand is rehybridized to an sp^2-like orbital which is directed along the S−S direction, while the other remains as an almost pure p-orbital. As in the case of type 1 centers, transitions from the thiolate σ-orbitals to the SOMO are expected to be too high in energy to contribute to the absorption spectrum in the visible region.

Model studies have shown that charge transfer (CT) transitions from imidazole π-orbitals to the SOMO occur in the region around 33 000 cm^{-1} with extinction coefficients of usually <500 M^{-1} cm^{-1} in cupric complexes.[74] Thus, these transitions are unlikely to be observed in the present case, since they will be either outside the accessible spectral range or obscured by the much more intense transitions within the Cu_2S_2 core. This also excludes the Cu−N σ-bonding orbitals from consideration in the interpretation of the Cu_A absorption spectrum. Initial calculations were performed with imidazole instead of NH_3, but this did not change any of the principal conclusions.

Thus, the minimal model required for the interpretation of the optical properties of Cu_A consists of the set of 10 copper d-orbitals and four in-plane thiolate orbitals. Fragment orbitals of the same symmetry species can combine which each other to form MOs. The quantitative composition of the MOs cannot be inferred from group theory, but requires a careful analysis of experimental data coupled with theoretical calculations. As has been pointed out elsewhere[20,55] and will be emphasized below, the degree of mixing between copper and sulfur fragment orbitals is almost complete, whereas the nitrogen donor orbitals

(66) Salahub, D. R.; Zerner, M. C. In *The Challenge of d and f Electrons: Theory and Computation*; Salahub, D. R., Zerner, M. C., Eds.; ACS Symposium Series 394; American Chemical Society: Washington, DC, 1989; pp 1−16.

(67) Guckert, J. A.; Lowery, M. D.; Solomon, E. I. *J. Am. Chem. Soc.* **1995**, *117*, 2817−2844.

(68) Solomon, E. I.; Penfield, K. W.; Wilcox, D. E. *Struct. Bonding* **1983**, *53*, 1−57.

(69) Solomon, E. I.; Baldwin, M. J.; Lowery, M. D. *Chem. Rev.* **1992**, *92*, 521−542.

(70) Solomon, E. I.; Lowery, M. D. *Science* **1993**, *259*, 1575−1581.

(71) Solomon, E. I.; Lowery, M. D. In *The Chemistry of Copper and Zinc Triads*; Welch, A. J., Chapman, S. K., Eds.; The Royal Society of Chemistry: Cambridge, England, 1993; pp 12−29.

(72) Solomon, E. I.; Hemming, B. L.; Root, D. E. In *Bioinorganic Chemistry of Copper*; Karlin, K. D., Tyeklar, Z., Eds.; Chapman & Hall: New York, 1992; pp 3−20.

(73) Solomon, E. I.; Gewirth, A. A.; Cohen, S. L. In *Understanding Molecular Properties*; Avery, J., Dahl, J. P., Hansen, A. E., Eds.; D. Reidel: Dordrecht, The Netherlands, 1987; pp 27−68.

(74) Schugar, H. J. In *Copper Coordination Chemistry: Biochemical and Inorganic Perspectives*; Karlin, K. D., Zubieta, J., Eds.; Adenine Press: New York, 1982; pp 43−74.

Table 3. Calculated Spin and Charge Distribution in the Various Excited States of Cu_A[a]

band	symmetry	one-electron excitation	q_{Cu}	ρ_{Cu}	q_S	ρ_S	q_N	ρ_N
GS	B_{3u}	−	0.118	0.181	−0.209	0.279	−0.148	0.018
1	B_{2u}	$2b_{2u} \rightarrow 3b_{3u}$	0.158	0.221	−0.225	0.264	−0.165	0.001
2	A_g	$3a_g \rightarrow 3b_{3u}$	0.092	0.157	−0.190	0.296	−0.160	0.006
3	B_{1g}	$2b_{1g} \rightarrow 3b_{3u}$	0.125	0.189	−0.213	0.274	−0.164	0.002
4	B_{3u}	$2b_{3u} \rightarrow 3b_{3u}$	0.384	0.446	−0.471	0.018	−0.139	0.027
5	A_u	$1a_u \rightarrow 3b_{3u}$	0.473	0.498	−0.489	0.001	−0.166	0.000
6	B_{2g}	$1b_{2g} \rightarrow 3b_{3u}$	0.370	0.432	−0.433	0.057	−0.165	0.001
7	B_{3g}	$1b_{3g} \rightarrow 3b_{3u}$	0.389	0.451	−0.460	0.030	−0.162	0.004
8	B_{1u}	$1b_{1u} \rightarrow 3b_{3u}$	0.308	0.371	−0.383	0.106	−0.165	0.001
9	B_{1g}	$1b_{1g} \rightarrow 3b_{3u}$	0.350	0.414	−0.415	0.071	−0.165	0.001
10	A_g	$1a_g \rightarrow 3b_{3u}$	0.389	0.451	−0.484	0.006	−0.128	0.037
11	B_{3u}	$1b_{3u} \rightarrow 3b_{3u}$	0.297	0.360	−0.384	0.104	−0.158	0.008
12	A_g	$2a_g \rightarrow 3b_{3u}$	0.306	0.373	−0.390	0.094	−0.153	0.014
13	B_{2u}	$1b_{2u} \rightarrow 3b_{3u}$	0.295	0.364	−0.372	0.110	−0.165	0.001

[a] All values for partial charges (q_x) and spin populations (ρ_X) refer to a population analysis in the zero-differential overlap basis and were obtained from the ROHF-INDO/S-CIS wave function.

make only small contributions (Table 3). As shown by the INDO/S calculations, the MOs can be conveniently subdivided into three groups: a group of four orbitals which are antibonding with respect to copper and sulfur, a group of four orbitals which are bonding with respect to copper and sulfur, and a group of six nonbonding orbitals which are essentially metal in character. (See Figure 6B.) As we show in the following paragraphs, this set of 14 orbitals represents the minimum model which is necessary for a detailed interpretation of the spectroscopic findings. While one would intuitively expect the nonbonding orbitals to lie between the antibonding and the bonding set, the analysis indicates that exceptions to this expectation are possible.

B. Choice of Ground State. In the MV state $[N_{His}Cu(S_{Cys})_2CuN_{His}]^+$, the total electron spin is $^1/_2$, and all orbitals except for the highest one are doubly occupied. The choice of ground state is ambiguous, and both $3b_{3u}$ and $2b_{2u}$ in Figure 6 are plausible choices for the SOMO. Consistent with the arguments in refs 20 and 55, the $^2B_{3u}$ state was chosen as the ground state, and we will show later that this choice is consistent with the magneto-optical data. The calculated absorbance and MCD spectra show similar qualitative features for both ground states. However, the experimental data are easier to reconcile for a $^2B_{3u}$ ground state than for a $^2B_{2u}$ ground state.

C. Group Theoretical Analysis of Electric and Magnetic Dipole Transitions. Under D_{2h} symmetry there is a theoretical maximum of 10 transitions from the 13 doubly occupied MOs in Figure 6 into the $3b_{3u}$ SOMO, six of which would be electric dipole allowed, and hence MCD active, and four of which would be magnetic dipole allowed. Transitions from the SOMO to unoccupied orbitals or even from doubly occupied to unoccupied orbitals are not expected to be important since the reduced Cu_A site is colorless. Indeed, configurations of this type are found at much higher energies in our INDO/S calculations. There is no degenerate transition which would be intrinsically allowed in two directions. Intense MCD C-terms can only arise if a transition is allowed in two perpendicular directions. Consequently the strong MCD C-term intensity observed experimentally must be allowed by out-of-state spin−orbit coupling between states of suitable symmetry in close energetic proximity. These states are expected to be formed from strongly mixed copper and sulfur orbitals, in order for the spin−orbit coupling to be effective. Equally, in order to observe intense CD bands, the transitions need to be simultaneously electric dipole and magnetic dipole allowed, a situation which would only exist in much lower symmetry point groups. However, it is frequently the case that magnetic dipole transitions which gain weak electric dipole intensity by some borrowing mechanism give rise to strong CD bands. Therefore it can be argued that D_{2h} is still a good choice of point group for analysis of the spectra since any point group which formally allows a transition to be simultaneously electric dipole and magnetic dipole allowed also lacks a center of inversion and would thus result in all the transitions being present in both the CD and MCD spectra, a situation which clearly does not exist in the experimental data of Figures 3−5.

Assignment of Experimental Spectra

A typical way to assign the optical spectra of transition metal complexes is to divide them into a CT and a d−d region. Even without the high degree of covalency shown to be present in the Cu_A center, in a dimer containing a center of inversion, it might be expected that there will be 10 orbitals formed from the d-sets of the two metal ions. Five of these symmetry orbitals will have even and five odd symmetry. This means that in the absence of strong mixing between metal and ligand or metal d/p functions, there are Laporte-allowed d−d transitions which can gain considerable intensity. For nonbridged MV copper dimers, this behavior is exemplified by the cryptate complexes.[75] In such a case it becomes difficult to use intensity arguments alone to assign specific transitions as d−d or CT. Before discussing the detailed spectroscopic assignments, it is interesting to compare the ground state charge distribution with the electron and spin distributions in the various excited states. From the data in Table 3 it can be seen that very little charge rearrangement occurs during optical excitation. It is clear that the term "charge transfer transition" is inappropriate to describe the nature of optical excitations in the Cu_A center. The calculated charge for the two excited states which make up the "purple band", $^2B_{1g}$ and ^2A_g (vide infra), is in fact more positive for the copper ions than for the ground state $^2B_{3u}$, which means that the transitions are, if anything, metal-to-ligand CT rather than ligand-to-metal CT. However, the amount of charge transfer is too small to justify either of these terms.

Resonance Raman (RR) data for several Cu_A-containing proteins show that there is strong enhancement of the Cu−S vibrational modes within the Cu_A chromophore bands.[76,77] Excitation profile data on the soluble Cu_A domain from *B. subtilis* has shown that there is enhancement of copper−sulfur vibrations throughout the optical spectrum from approximately

(75) Farrar, J. A.; McKee, V.; Al-Obaidi, A. H. R.; McGarvey, J. J.; Nelson, J.; Thomson, A. J. *Inorg. Chem.* **1995**, *34*, 1302−1303.

(76) Andrew, C. R.; Han, J.; de Vries, S.; van der Oost, J.; Averill, B. A.; Loehr, T. M.; Sanders-Loehr, J. *J. Am. Chem. Soc.* **1994**, *116*, 10805−10806.

(77) Andrew, C. R.; Lappalainen, P.; Saraste, M.; Hay, M. T.; Lu, Y.; Dennison, C.; Canters, G. W.; Fee, J. A.; Slutter, C. E.; Nakamura, N.; Sanders-Loehr, J. *J. Am. Chem. Soc.* **1995**, *117*, 10759−10760.

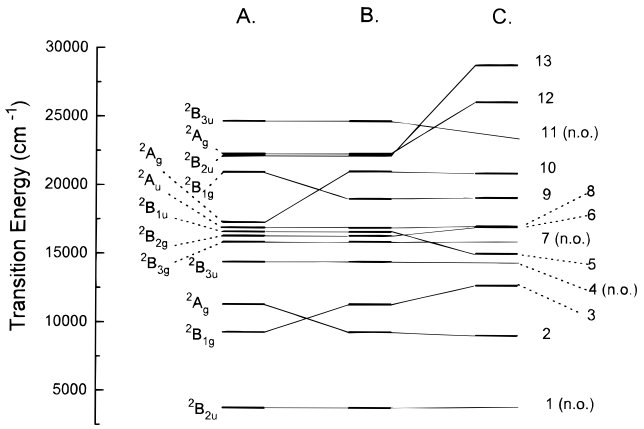

Figure 7. Energy level scheme showing calculated ordering of the states under D_{2h} symmetry and experimentally determined band positions for the Cu_A center in PdII. (A) Energy levels as calculated by the INDO/S-CIS method. (B) Calculated energy levels after the reordering of states suggested by the experimental data. (C) Experimentally assigned energy levels for the Cu_A center in PdII. The symmetry label on each state is that of the singly occupied orbital in the relevant excited state.

25 000 cm^{-1} downward;[76] indeed there may also be enhancement in electronic transitions above 25 000 cm^{-1}, but the RR data do not extend to higher energies. This requires that, at the very least, the bands numbered 2−13 in the experimental spectra of PdII Cu_A be assigned to transitions from the 13 Cu/S-based MOs below the SOMO, shown in Figures 6b and 7, to the $3b_{3u}$ SOMO.

A. Transitions from the Cu/S Antibonding Orbitals. The lowest energy transitions would be expected to occur within the Cu/S antibonding set of orbitals. Of these three transitions, two will be electric dipole allowed and the third will be magnetic dipole allowed. One parameter of paramount importance for the EPR and MCD properties of Cu_A is the amount of angular momentum in the ground state, which is induced by spin−orbit coupling to electronically excited states. The most important factor which controls the amount of angular momentum in the *z*-direction is the separation between the $^2B_{3u}$ ground state and the first excited state, $^2B_{2u}$.[20] In the present study we have adjusted this separation to give a reasonable fit to the ground state *g*-values. From simple considerations[20] an optimum value of ∼3500 cm^{-1} is obtained. This energy is too low for the transition to be observed experimentally by the instrumentation available to us. However, this allows the two lowest energy observed transitions, labeled 2 and 3, to be assigned to the oppositely polarized electric dipole allowed, the $3a_g \rightarrow 3b_{3u}$ and the $2b_{1g} \rightarrow 3b_{3u}$ transitions, respectively. These transitions have acquired some magnetic dipole character and hence are also observed in the CD spectra, Figures 3C and 4C. The exact assignment is based on two pieces of information. Firstly, in experiments on oriented membranes, only one of the three major bands present in the MCD spectrum, that at 460 nm, decreases in relative intensity, suggesting that it is the only transition polarized along the Cu−Cu (*x*) axis. This implies that band 3 is polarized along the S−S (*y*) axis. Secondly, the calculated relative intensities predict the $2b_{1g} \rightarrow 3b_{3u}$ transition to be much more intense than the $3a_g \rightarrow 3b_{3u}$ transition. Hence, band 2 is assigned to $3a_g \rightarrow 3b_{3u}$, and band 3 is assigned to $2b_{1g} \rightarrow 3b_{3u}$, Figure 7C. This is the reverse of the order suggested by the INDO/S method, Figure 7A.

B. Transitions from the Cu/S Bonding Orbitals. The lowest lying orbitals and hence highest energy transitions may be expected to be from the Cu/S bonding orbitals to the $3b_{3u}$ SOMO. From these four orbitals there will be two electric dipole allowed, one magnetic dipole allowed, and one forbidden transitions. These may also be expected to be intense transitions since they are polarized in the plane of the Cu_2S_2 rhomb. These criteria are met by bands 9 and 10, which are assigned to the oppositely polarized electric dipole allowed transitions, $1b_{1g} \rightarrow 3b_{3u}$ and $1a_g \rightarrow 3b_{3u}$. The INDO/S calculations would put the *y*-polarized $1b_{1g} \rightarrow 3b_{3u}$ transition at higher energy than the *x*-polarized $1a_g \rightarrow 3b_{3u}$ transition, Figure 7A. However, reference to the oriented membrane data from COX shows that the negative band in the MCD spectrum at approximately 21 000 cm^{-1} must be polarized along the metal−metal bond, or along the *x*-axis, Figure 6. This puts the experimentally observed $1a_g \rightarrow 3b_{3u}$ transition, Figure 7C, at higher energy in contrast to the calculated order. The magnetic dipole allowed transition $1b_{2u} \rightarrow 3b_{3u}$ has been calculated to lie at slightly higher energy, and thus band 13 is assigned to this transition. The fourth transition from this subset of orbitals, $1b_{3u} \rightarrow 3b_{3u}$, is formally forbidden under D_{2h} symmetry. It is of interest to note that of the two electric dipole allowed transitions, 9 and 10, only band 9 exhibits any magnetic dipole character. This may be ascribed to the fact that this transition, which is polarized along the S−S axis, may acquire some magnetic dipole character along the *y*-axis due to the twist of the two $-CH_2-S^-$ bonds about this axis; see Figure 1B.

C. Transitions from the Copper Nonbonding Orbitals. Of the maximum number of six transitions from the nonbonding orbitals, two are formally forbidden, two are magnetic dipole allowed, and two are electric dipole allowed. Bands 5 and 8, observed with opposite signs in the CD spectrum, have very little intensity in the UV-vis spectrum and are therefore assigned to the oppositely polarized, magnetic dipole allowed transitions $1a_u \rightarrow 3b_{3u}$ and $1b_{1u} \rightarrow 3b_{3u}$, Figure 7. By contrast the Kuhn anisotropy factors[51] for bands 2, 3, and 9 are far too small for these transitions to be magnetic dipole allowed; see Table 1. Calculations suggest that the electric dipole allowed transition $2a_g \rightarrow 3b_{3u}$ from the nonbonding set occurs at higher energy than the transitions from the Cu/S bonding orbitals, Figure 7A. Thus, this transition is assigned to band 12, observed in the MCD spectrum of PdII. This leaves band 6 in the experimental spectrum to be assigned to the electric dipole allowed *z*-polarized transition $1b_{2g} \rightarrow 3b_{3u}$. According to our INDO/S calculations, band 6 would be interpreted as a composite band made up of the $1b_{2g} \rightarrow 3b_{3u}$ and the formally forbidden $1b_{3g} \rightarrow 3b_{3u}$ transition. There are two mechanisms which could introduce electric dipole intensity in the latter transition. First, the $^2B_{2g}$ and $^2B_{3g}$ states are of suitable symmetry to be mixed by spin−orbit coupling, and second, the calculation indicates that the drop in symmetry ($D_{2h} \rightarrow C_i$) results in a strong mixing between the $^2B_{1g}$ and $^2B_{3g}$ states. Thus, the $1b_{3g} \rightarrow 3b_{3u}$ transition would borrow intensity from two allowed transitions.

These assignments are summarized in Table 4. All the expected transitions within the Cu/S manifold are accounted for. Figure 7 compares the calculated transition energies, Figure 7A, with those determined experimentally, Figure 7C, and explicitly shows the fitting of the calculated transition energies required to match the experimental data, Figure 7B. Figure 8 shows the simulated absorbance and MCD spectra, obtained using the energy level ordering shown in Figure 7B. It is seen that there is good correspondence between the spectra calculated by the INDO/S method and the experimental spectra. Especially, the MCD spectrum is well accounted for in terms of the intense C-terms displayed by the major transitions. However, two important reversals of states have occurred in the calculations, and they have been artificially corrected in the simulation in Figure 8. As shown in the

Table 4. Details of the Calculated Absorption and MCD Spectra, Presented in Figure 8, for a Model in C_i Symmetry by the ROHF-INDO/S-CIS Method[a]

band	excited state symmetry	one-electron excitation	% purity	pol[b]	f_{osc} (calc)	f_{osc} (obs)	$\bar{C}_0/\bar{D}_0$ (calc)	$\bar{C}_0/\bar{D}_0$ (obs)
1	B_{2u}	$2b_{2u} \rightarrow 3b_{3u}$	97	m.d.				
2	A_g	$3a_g \rightarrow 3b_{3u}$	88	X	0.008	0.0031	−0.308	−0.183
3	B_{1g}	$2b_{1g} \rightarrow 3b_{3u}$	97	Y	0.105	0.0224	−0.180	−0.334
4	B_{3u}	$2b_{3u} \rightarrow 3b_{3u}$	97	F				
5	B_{1u}	$1b_{1u} \rightarrow 3b_{3u}$	100	m.d.				
6	B_{2g}	$1b_{2g} \rightarrow 3b_{3u}$	62	Z	0.006	0.0124	−0.063	0.0330
7	B_{3g}	$1b_{3g} \rightarrow 3b_{3u}$	95	F(XY)	0.018	n.o.[c]	0.006	n.o.
8	A_u	$1a_u \rightarrow 3b_{3u}$	79	m.d.				
9	B_{1g}	$1b_{1g} \rightarrow 3b_{3u}$	60	Y	0.134	0.0159	0.598	1.1774
10	A_g	$1a_g \rightarrow 3b_{3u}$	92	X	0.078	0.0427	−0.473	−0.383
11	B_{3u}	$1b_{3u} \rightarrow 3b_{3u}$	95	F				
12	A_g	$2a_g \rightarrow 3b_{3u}$	83	X	0.005	0.0084	−0.100	0.0003
13	B_{2u}	$1b_{2u} \rightarrow 3b_{3u}$	77	m.d.				

[a] Prior to the inclusion of spin−orbit coupling and calculation of UV and MCD intensities, the following changes were made: (a) states 2 and 3 (B_{1g} and A_g) were swapped, and (b) states 9 and 10 (A_g and B_{1g}) were swapped and were set from 17 300 and 20 950 cm^{-1} to 21 000 and 19 000 cm^{-1}, respectively (see Figure 7). The calculated intensities are from a calculation including spin−orbit coupling. [b] m.d. = magnetic dipole allowed; F = forbidden. [c] n.o. = not observed.

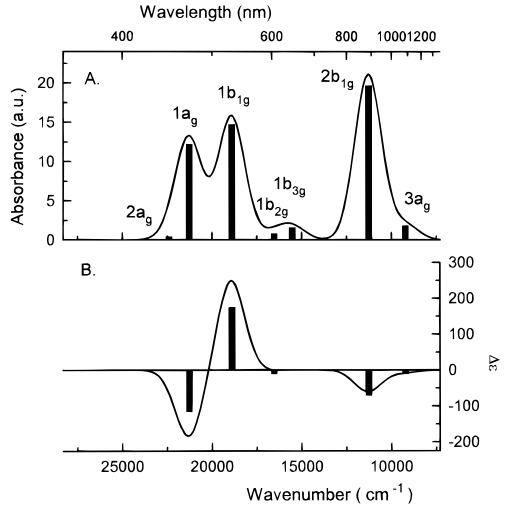

Figure 8. Absorbance and MCD spectra calculated by the INDO/S-CIS method as described in subsection D of the Experimental Methods section. Two state reversals as indicated in Figure 7B were made to match the experimental data, and the first excited $^2B_{2u}$ state was adjusted to 3750 cm^{-1} in order to fit the experimental *g*-values. The symmetry label on each transition in the absorbance spectrum indicates the symmetry of the singly occupied orbital in the relevant excited state.

Appendix, this reversal is not necessary to arrive at the correct description of the MCD spectrum, but is required to fit the polarization information provided by the experimental data on oriented membranes.

D. Assignment of the Cu_A* Spectra. The optical spectra of the Cu_A* center are remarkably different from those of Cu_A. Although the symmetry of the structure, excluding consideration of M218 and E209, approximates to C_{2h}, the partial localization of the copper valencies demonstrated by the EPR spectrum implies that the center of inversion is absent. The loss of the center of inversion lowers the true symmetry at least to C_2, and the parity restrictions on the selection rules will be relaxed to some further degree. However, taking the highest possible symmetry of the Cu_2S_2 entity, C_{2h}, allows assignment of the optical spectra. As the symmetry drops from D_{2h} to C_{2h}, three formally forbidden transitions under D_{2h}, from the Cu/S bonding orbitals, $1b_{3u} \rightarrow 3b_{3u}$, and from the Cu nonbonding orbitals, $1b_{3g} \rightarrow 3b_{3u}$ and $2b_{3u} \rightarrow 3b_{3u}$, become allowed. Under C_{2h} these would be $2b_u \rightarrow 5b_u$, $1b_g \rightarrow 5b_u$, and $3b_u \rightarrow 5b_u$, respectively. Two of these transitions are observed in the optical spectra of purple CyoA. Band 11 in the CD spectrum of purple CyoA is assigned to the magnetic dipole allowed $2b_u \rightarrow 5b_u$ transition, and band 7 in the MCD spectrum is assigned as the electric dipole allowed $1b_g \rightarrow 5b_u$ transition. The magnetic dipole allowed $3b_u \rightarrow 5b_u$ transition remains unobserved in the experimental CD spectrum of purple CyoA, possibly due to low intensity.

Discussion

This work has given a detailed description of the excited states of Cu_A, a MV thiolate-bridged dinuclear copper center. Two forms of the chromophore have been studied. One form, Cu_A, is found in the enzyme nitrous oxide reductase lacking its catalytic center, and in the soluble domain of subunit II of *P. denitrificans* COX, and exists in a MV [Cu(I),Cu(II)] ground state in which the unpaired electron density is equally shared by the two copper ions, as shown by the copper hyperfine parameters of the EPR spectra. The optical absorption, MCD, and CD spectra attest to a very close structural similarity between the Cu_A centers in these two enzymes in spite of considerable sequence differences in the protein environment of the second coordination sphere. In the second form, Cu_A*, the copper ions have become slightly inequivalent, evident from the copper hyperfine coupling constants in the EPR spectrum at X-band. This partial trapping of the valences causes changes in state energies and results in substantial redistribution of intensity within the optical spectra.

By combining the results from absorption spectroscopy, CD spectroscopy, and low-temperature MCD spectroscopy of isotropic and partially oriented samples together with theoretical simulations of the spectra, an assignment has been proposed. The analysis of the MCD spectrum of the Cu_A chromophore has relied in part on the use of a theoretical simulation based on the INDO/S method, developed by Zerner and co-workers,[53,54,78] which has been extended for the calculation of MCD C-term intensities and signs. The method has been tested against the absorbance and MCD spectra of well-characterized cupric complexes, including $[CuCl_4]^{2-}$, with satisfactory results. Previously, assignments of optical spectra using this method have given encouraging results in a variety of transition metal systems, including thioether complexes,[79−81] hexaquo com-

(78) Bacon, A.; Zerner, M. C. *Theor. Chim. Acta* **1979**, *53*, 21−54.
(79) Krogh-Jespersen, K.; Westbrook, J. D.; Potenza, J. A.; Schugar, H. J. *J. Am. Chem. Soc.* **1987**, *109*, 7025−7031.
(80) Krogh-Jespersen, K.; Zhang, X. E.; Westbrook, J. D.; Fikar, R.; Nayak, K.; Kwik, W. L.; Potenza, J. A.; Schugar, H. J. *J. Am. Chem. Soc.* **1989**, *111*, 4082−4091.
(81) Krogh-Jespersen, K.; Zhang, X.; Ding, Y.; Westbrook, J. D.; Potenza, J. A.; Schugar, H. J. *J. Am. Chem. Soc.* **1992**, *114*, 4345−4353.

plexes,[82] metalated planar macrocycles,[83−88] carbonyl complexes,[89,90] and amine complexes.[91,92] Although the method has not previously been applied either to highly covalent MV transition metal dimers or to the calculation of MCD spectra, a MO model is expected to lead to a more reliable interpretation than previous ligand field treatments which ignore covalency and model CT transitions as pure metal d → p transitions.[93,94] The results obtained in this study for the rather complex structure of the Cu_A center show that, when used in conjunction with experimental data, a suitably parameterized model is of considerable help in the assignment of experimental spectra.

The interpretation of the electronic spectra has been made in terms of a covalent, planar core, $[Cu_2(SR)_2]^+$, with Cu−S distances of ∼2.2 Å, a Cu−Cu distance of 2.5 Å, and a Cu−S−Cu angle of 70°. The 14 energy levels which arise from five 3d-orbitals on each copper ion and two lone pair thiolate orbitals on each cysteine ligand divide into three sets, four at lowest energy which are bonding with respect to the Cu−S interaction, and four at highest energy which are antibonding with respect to the Cu−S interaction. These two sets of four orbitals hold the key to the assignment. The third group of orbitals are essentially copper 3d-orbitals and are nonbonding with respect to copper and sulfur.

The apparently rather simple absorption spectrum of Cu_A is dominated by a pair of intense transitions, bands 9 and 10, at 525 and 475 nm and a broader less intense transition, band 3, at 830 nm. All three transitions are polarized approximately in the plane of the Cu_2S_2 rhomb, those at 525 and 830 nm being polarized parallel to the S−S axis and the band at 475 nm being polarized along the Cu−Cu axis. Since the equivalence of the valencies imposes a spectroscopic center of inversion on the Cu_2S_2 rhomb, all states are classified as either even (g) or odd (u) with respect to the center, and transitions are either electric dipole or magnetic dipole allowed. The major spectral features may be understood by reference to Figure 9, which shows two sets of four orbitals, bonding and antibonding with respect to the Cu−S interactions. There are two pairs of perpendicularly polarized electric dipole transitions, 9, 10 and 2, 3. The two highest energy transitions, 9 and 10, are separated by only 1800 cm^{-1} and give rise, via spin−orbit mixing, to a pair of oppositely signed MCD C-terms, Table 4. Copper−sulfur covalence ensures that the orbitals have a high copper character and hence substantial spin−orbit coupling. These interactions sustain orbital angular momentum in this pair of states and hence lead to the characteristic MCD shape. A second pair of transitions, 2 and 3, are expected within the antibonding set of orbitals.

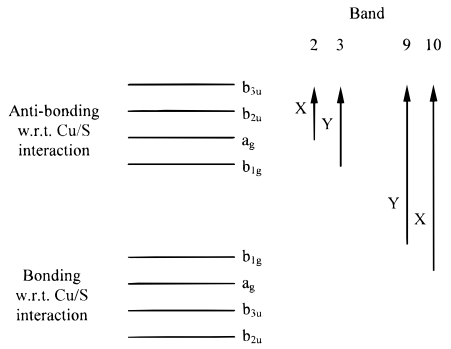

Figure 9. Schematic to show the assignment of the four major bands in the optical spectra of Cu_A.

Again, because of the high covalence, these transitions have considerable intensity and are expected to give rise to oppositely signed C-terms. However, both carry the same sign C-term. The influence of a significant orbital moment in the ground state due to SOC between the ground state and $^2B_{2u}$ excited state, predicted to lie at 3500 cm^{-1}, gives rise to C-terms of the same sign within these two transitions—see Appendix for a detailed description.

Relaxation of the selection rules is observed in the Cu_A* center in which the valencies become partially trapped. Lacking a strict center of inversion, intensity is spread throughout many more transitions. As a result, the spectrum of Cu_A* appears at first sight to be more complex with an overall lower intensity. However, we have demonstrated a one-to-one correspondence between the transitions in the spectra of Cu_A and Cu_A*. The question arises as to the source of the partial valence trapping in the case of Cu_A*. The structure of this center shows the carbonyl oxygen atom of E209 to be within a bonding distance of one copper ion, whereas in the case of the Cu_A structure in COX, this atom is at a longer distance. Therefore it is natural to propose that the approach of the E209 carbonyl oxygen is responsible for the partial valence localization. The Cu_A center can also be switched to a fully trapped state by making the coordination site of one copper ion very different from that of the other. This has been achieved for Cu_A in PdII either by removal of one of the terminal histidine residues through the mutation H224N or by loss of H224 which occurs at high pH.[43]

For the delocalized Cu_A center, an interesting comparison with the theories of "resonance delocalization" or "double exchange" mechanisms can be made now that a complete assignment of the optical spectrum has been achieved. In phenomenological theories of valence delocalization, two localized states combine to form delocalized states by means of double exchange interaction.[95−100] At the point of avoided crossing of the potential energy surfaces, the states are delocalized and the energy separation of these two states is given by the quantity $2|B|$, where B is a measure of the delocalization energy. The connection to a many electron model as presented here can be made by comparing this energy to the one-electron excitation from the symmetric to the antisymmetric orbital combination, which in the present case is the $3a_g \rightarrow 3b_{3u}$ transition occurring at ∼9000 cm^{-1}. Thus, we arrive at an estimate of 4500 cm^{-1}

(82) Anderson, W. P.; Edwards, W. D.; Zerner, M. C. *Inorg. Chem.* **1986**, *25*, 2728−2732.
(83) Edwards, W. D.; Weiner, B.; Zerner, M. C. *J. Phys. Chem.* **1988**, *92*, 6188−6197.
(84) Edwards, W. D.; Weiner, B.; Zerner, M. C. *J. Am. Chem. Soc.* **1986**, *108*, 2196−2204.
(85) Edwards, W. D.; Zerner, M. C. *Can. J. Chem.* **1985**, *63*, 1763−1772.
(86) Loew, G. H.; Herman, Z. S.; Zerner, M. C. *Int. J. Quantum Chem.* **1980**, *18*, 481.
(87) Edwards, W. D.; Zerner, M. C. *Int. J. Quantum Chem.* **1983**, *23*, 1407−1432.
(88) Cory, M. G.; Hirose, H.; Zerner, M. C. *Inorg. Chem.* **1995**, *34*, 2969−2979.
(89) Kotzian, M.; Rosch, N.; Schroder, H.; Zerner, M. C. *J. Am. Chem. Soc.* **1989**, *111*, 7687−7696.
(90) Merz, K. M.; Hoffmann, R. *Inorg. Chem.* **1988**, *27*, 2120−2127.
(91) Shin, Y. K.; Brunschwig, B. S.; Creutz, C.; Newton, M. D.; Sutin, N. *J. Phys. Chem.* **1996**, *100*, 1104−1110.
(92) Stavrev, K. K.; Zerner, M. C. *J. Am. Chem. Soc.* **1995**, *117*, 8684−8685.
(93) Gerstman, B. S.; Brill, A. S. *J. Chem. Phys.* **1985**, *82*, 1212−1230.
(94) Landrum, G. A.; Ekberg, C. A.; Whittaker, J. W. *Biophys. J.* **1995**, *69*, 674−689.
(95) Piepho, S. B.; Krausz, E. R.; Schatz, P. N. *J. Am. Chem. Soc.* **1978**, *100*, 2996−3005.
(96) Schatz, P. N. In *Mixed Valence Compounds*; Brown, R. D., Ed.; D. Reidel: Dordrecht, The Netherlands, 1980; pp 115−150.
(97) Wong, K. Y.; Schatz, P. N.; Piepho, S. B. *J. Am. Chem. Soc.* **1979**, *101*, 2793−2803.
(98) Anderson, P. W.; Hasegawa, H. *Phys. Rev.* **1955**, *100*, 675−681.
(99) Zhang, L. T.; Ko, J.; Ondrechen, M. J. *J. Am. Chem. Soc.* **1987**, *109*, 1666−1671.
(100) For a review, see: Blondin, G.; Giererd, J.-J. *Chem. Rev.* **1990**, *90*, 1359−1376.

for the absolute value of *B*. This is at least 1 order of magnitude larger than the energy of the vibrations of the Cu_2S_2 core (shown to be of the order of 400 cm^{-1} by RR spectroscopy[76]), which would favor localization by means of vibronic coupling.[95] Hence, the strong intersite interaction due to the dithiolate bridges must be responsible for the valence delocalization in Cu_A. It is of interest to compare the Cu_A thiolate-bridged MV dimer with the iron−sulfur clusters in which a delocalized Fe(II)Fe(III) pair of maximal spin exists. A minimum value for *B* of 1200 cm^{-1} has been suggested for electron delocalization to occur, and theoretical calculation gives values of between 2000 and 4500 cm^{-1} for the delocalization energy.[101]

Copper ions coordinated by a set of thiolate ligands, as for example in the case of copper metallothionein in which the copper is coordinated by up to three bridged and terminal thiolate groups, are held in the +1 oxidation state. No reversible oxidation of Cu(I) in metallothionein has been reported. Mononuclear copper(II) thiolate and bisthiolate coordination is well established in type 1 blue copper proteins and in copper substituted into the catalytic site of liver alcohol dehydrogenase. Both sites allow reversible redox cycling Cu(I)/Cu(II). The structure of Cu_A is a further variant in which sets of thiolate and histidine ligands allow a one-electron cycle [Cu(II)/Cu(I)] to [Cu(I)/Cu(I)] to take place at a potential of +250−280 mV.[102] No successful attempts to oxidize Cu_A *reversibly* to [Cu(II)/Cu(II)] have been reported so far. Models for the Cu_A site which possess a planar bisthiolate-bridged dinuclear copper fragment include a complex with 2,9-substituted 1,10-phenanthroline ligands on each copper to generate a pseudotetrahedral site.[103,104] Copper−copper distances varying between 2.613 and 3.019 Å were reported, depending on the 2,9-substituents. However, this complex exists in the [Cu(I),Cu(I)] form and can only be irreversibly oxidized. The strong field ligand coordination may account for this. A more recent report is of a dinuclear copper complex with a pair of thiolate bridges and terminal coordination by diazoalkyl bridges, with a Cu−Cu distance of 2.93 Å. This complex generates two voltametric waves at −500 and +350 mV in methanol, although the reduction is irreversible and the oxidation is reversible only at high scan rates.[105]

The relative orbital energies proposed here and elsewhere[20,55] show that the odd electron of the MV form of Cu_A is in an orbital which is strongly antibonding with respect to the copper−thiolate interaction. Hence, this implies that the orbitals shown in Figure 6B are not primarily responsible for the stability of the complex, and in the fully reduced form, they are even less so. Hence, low-lying thiolate 3d-orbitals and empty copper 4s- and 4p-orbitals must play a role in stability.[55,106] The near planarity of the $Cu_2S_2N_2$ unit may be an important requirement for the reversibility of the [Cu(I),Cu(I)]/[Cu(II),Cu(I)] couple.

The $[Cu_2(SR)_2]$ unit is appropriate to serve as an electron transfer center in biology. The $[Cu_2S_2]$ rhomb is highly covalent. An electron added to the unit is delocalized over at least four atoms so the reorganization energy will be low.[107] The plane of the rhomb sits almost vertically above hemes *a* and a_3 in COX in the membrane. The electron donor, cytochrome *c*, is thought to dock with subunit II at sites adjacent to the copper center.[108] The $[Cu_2S_2]$ rhomb hence provides an effective pathway for an electron across subunit II toward hemes *a* and a_3. At present the evidence points to Cu_A as a one-electron storage reagent in COX. However, bacterial quinone oxidases have remarkable sequence and hence structural homology with COX. The quinol can donate two electrons via a semiquinone form which is unstable with respect to its oxidized and reduced states. There is a formal similarity between the three oxidation states of Cu_A, [Cu(I)/Cu(I)], [Cu(I)/Cu(II)], and [Cu(II)/Cu(II)], and the three oxidation states of quinol, QH_2, semiquinone, SQ, and quinone, Q. It remains to be shown under circumstances of turnover how many electrons Cu_A can donate to the cytochromes of COX.

Acknowledgment. Financial support is acknowledged from the Biological and Biochemical Sciences Research Council via funding of the Centre for Metalloprotein Spectroscopy and Biology (A.J.T., J.A.F.), from the European Union via the MASIMO program (A.J.T., J.A.F., P.M.H.K.), from the Deutsche Forschungsgemeinschaft (W.G.Z., P.M.H.K.), and from Fonds der Chemischen Industrie (W.G.Z.). P.L. was supported by a grant from the Academy of Finland. A.J.T., F.N., and J.A.F. would like to express thanks to Dr. Roger Grinter (UEA) for the many helpful discussions without which this project would not have been as successful. We thank Dr. Graham George for communicating his results on the Q-band EPR of oriented membranes of COX prior to publication.

Appendix

A striking feature of the assignment developed in the present paper is the fact that there are two pairs of transitions with symmetries $B_{1g} \rightarrow B_{3u}$ and $A_g \rightarrow B_{3u}$ and polarized along the *x*- and *y*-axes, respectively. However, one pair (bands 9 and 10) is associated with oppositely signed MCD C-terms, while the second pair (bands 2 and 3) shows negative MCD C-terms for both transitions. In this Appendix a simple mathematical treatment is developed to account for the observed behavior.

We consider four states of symmetries, B_{3u}, B_{2u}, A_g, and B_{1g}. These states are coupled by the *z*-component of the spin−orbit coupling (SOC) operator

$$\langle {}^2B_{3u}+|H_{SO}|{}^2B_{2u}+\rangle \equiv -iL_1'$$

$$\langle {}^2A_g+|H_{SO}|{}^2B_{1g}+\rangle \equiv -iL_2'$$

Since SOC only connects states of like parity, each 4 × 4 matrix reduces to 2 × 2 matrices which are readily solved. Within each pair of states the Hamiltonian has the appearance

$$\mathbf{H} = \begin{pmatrix} 0 & -iL' \\ iL' & \Delta \end{pmatrix}$$

where *L* is the effective spin−orbit coupling and Δ is the state separation in the zero-SOC limit. We can redefine **H** to be in units of Δ and write

$$\mathbf{H} = \begin{pmatrix} 0 & -iL \\ iL & 1 \end{pmatrix}$$

where $L \equiv L'/\Delta$. The eigenstates are

(101) Santum, S. F.; Noodleman, L.; Case, D. A. In *The Challenge of d and f Electrons: Theory and Computation*; Salahub, D. R., Zerner, M. C., Eds.; ACS Symposium Series 394; American Chemical Society: Washington, DC, 1989; pp 366−377.
(102) Malmström, B. G. *Q. Rev. Biophys.* **1973**, *6*, 389−432.
(103) Chadha, R. K.; Kumar, R.; Tuck, D. G. *Can. J. Chem.* **1987**, *65*, 1336−1342.
(104) Stange, A.; Kaum, W. *Z. Naturforsch., B: Chem. Sci.* **1995**, *50*, 115.
(105) Houser, R. P.; Young, V. G., Jr.; Tolman, W. B. *J. Am. Chem. Soc.* **1996**, *118*, 2101−2102.
(106) Mehrotra, P. K.; Hoffmann, R. *Inorg. Chem.* **1978**, *17*, 2187−2189.
(107) Larsson, L.; Källebring, B.; Wittung, P.; Malmström, B. *Proc. Natl. Acad. Sci. U.S.A.* **1995**, *92*, 7167−7171.
(108) Lappalainen, P.; Watmough, N. J.; Greenwood, C.; Saraste, M. *Biochemistry* **1995**, *34*, 5824−5830.

$$|0'\rangle = \mathrm{i}a|0\rangle + b|1\rangle$$

$$|1'\rangle = \mathrm{i}c|0\rangle + d|1\rangle$$

where

$$a = \frac{\sqrt{2}}{2}\frac{(1+\sqrt{1+4L_2})}{\sqrt{1+4L^2+\sqrt{1+4L^2}}}$$

$$b = \sqrt{2}\frac{L}{\sqrt{1+4L^2+\sqrt{1+4L^2}}}$$

$$c = \frac{\sqrt{2}}{2}\frac{(1-\sqrt{1+4L^2})}{\sqrt{1+4L^2}-\sqrt{1+4L^2}}$$

$$d = \sqrt{2}\frac{L}{\sqrt{1++4L^2}-\sqrt{1+4L^2}}$$

Thus, the spin−orbit-corrected ground state is written as

$$|^2\mathrm{B}_{3u}+'\rangle = \mathrm{i}\alpha|^2\mathrm{B}_{3u}+\rangle + \beta|^2\mathrm{B}_{2u}+\rangle$$

$$|^2\mathrm{B}_{3u}-'\rangle = -\mathrm{i}\alpha|^2\mathrm{B}_{3u}-\rangle + \beta|^2\mathrm{B}_{2u}-\rangle$$

and the components of the two spin-orbit-corrected excited states are

$$|^2\mathrm{A}_g+'\rangle = \mathrm{i}\gamma|^2\mathrm{A}_g\rangle + \delta|^2\mathrm{B}_{1g}+\rangle$$

$$|^2\mathrm{A}_g-'\rangle = -\mathrm{i}\gamma|^2\mathrm{A}_g-\rangle + \delta|^2\mathrm{B}_{1g}-\rangle$$

$$|^2\mathrm{B}_{1g}+'\rangle = i\gamma'|^2\mathrm{A}_g+\rangle\ \delta'|^2\mathrm{B}_{1g}+\rangle$$

$$|^2\mathrm{B}_{1g}-'\rangle = -\mathrm{i}\gamma|^2\mathrm{A}_g-\rangle + \delta'|^2\mathrm{B}_{1g}-\rangle$$

Defining

$$\langle \mathrm{B}_{3u}+|m|\mathrm{A}_g+\rangle = \mathrm{e}_x m_x$$

$$\langle \mathrm{B}_{3u}+m|\mathrm{B}_{1g}+\rangle = \mathrm{e}_y m_y$$

$$\langle \mathrm{B}_{2u}+|m|\mathrm{A}_g+\rangle = \mathrm{e}_y m'_y$$

$$\langle \mathrm{B}_{2u}+|m|\mathrm{B}_{1g}+\rangle = \mathrm{e}_x m'_x$$

the transition dipole matrix elements become:

$$\langle {}^2\mathrm{B}_{3u}+'|m|{}^2\mathrm{A}_g+'\rangle = \mathrm{e}_x(\alpha\gamma m_x + \beta\delta m'_x) + \mathrm{ie}_y(-\alpha\delta m_y + \beta\gamma m'_y)$$

$$\langle {}^2\mathrm{B}_{3u}+'|m|{}^2\mathrm{B}_{1g}+'\rangle = \mathrm{e}_x(\alpha\gamma' m_x + \beta\delta' m'_x) + \mathrm{ie}_y(-\alpha\delta' m_y + \beta\gamma' m'_y)$$

The transition moments for the spin-down transitions are the complex conjugate of this. Inserting into the general equation for $\bar{C}_0$, eq 1, we find

$$\bar{C}_0(\mathrm{B}_{3u}\rightarrow\mathrm{A}_g) = {}^1/_3 g_{zz}\{\gamma\delta[\alpha^2 m_x m_y - \beta^2 m'_x m'_y] + \alpha\beta[\delta^2 m'_x m_y - \gamma^2 m_x m'_y]\}$$

$$\bar{C}_0(\mathrm{B}_{3u}\rightarrow\mathrm{B}_{1g}) = {}^1/_3 g_{zz}\{\gamma'\delta'[\alpha^2 m_x m_y - \beta^2 m'_x m'_y] + \alpha\beta[\delta'^2 m'_x m_y - \gamma'^2 m_x m'_y]\}$$

Each of the C-terms have four contributions: (a) ${}^1/_3 g\gamma\delta\alpha^2 m_x m_y$—for appreciable excited state spin−orbit coupling, this is expected to be the leading term and is the only nonzero term in the absence of SOC with the ground state. The latter is very limited given the orbital component of the experimental *g*-values, $|L_1| \approx 0.2$. This term *must* give oppositely signed C-terms for the two transitions because $\gamma\delta = -\gamma'\delta'$. (b) ${}^1/_3 g\gamma\delta\beta^2 m_x m_y$—this term should always be much smaller than the first term since $\alpha^2 \gg \beta^2$. It may therefore be neglected in the discussion. In the limit of very effective excited state spin−orbit coupling (es-SOC), the transitions are expected to have large $\bar{C}_0/\bar{D}_0$ values which approach *g*/2. (c) ${}^1/_3 g\alpha\beta\gamma^2 m'_x m_y$ and (d) ${}^1/_3 g\alpha\beta\delta^2 m'_x m_y$—ground state SOC is required in order for $\alpha\beta$ to be nonzero. The relative magnitude of the terms depends on the details of the es-SOC. When es-SOC is zero ($L_2 \rightarrow 0$), $\gamma^2 \rightarrow 1$ and $\delta'^2 \rightarrow 1$. The relative C-term signs then depend on the relative signs of the transition moment products $m_x m'_y$ and $m_y m'_x$. For *equal* signs of $m_x m'_y$ the C-terms are opposite, and for *unequal* signs the C-terms are equal and may both be negative or positive. Furthermore, in this limit of zero es-SOC, these terms are expected to be dominant and to govern the overall signs of the C-terms. In this limit the transitions are expected to have $\bar{C}_0/\bar{D}_0$ values which are significantly smaller than 1.

We conclude that the origin of the oppositely signed C-terms in the purple band (bands 9 and 10) is excited state near degeneracy leading to a very effective excited state spin−orbit coupling ($|L_2| > 0.25$). On the other hand the two equally signed C-terms in bands 2 and 3 are due to reduction in excited state SOC caused by an energy state separation which is significantly larger than the effective SOC constant. The latter may also be reduced from the free ion value by extensive covalence. Thus, an excited state splitting of 3000 cm^{-1} or more is apparently sufficient to reduce the es-SOC sufficiently to bring the pair of transitions into the regime where the ground state spin−orbit coupling determines the C-term behavior. In order to have the two transitions with equal sign of C-term, it is required that the signs of the transition moment products are unequal ($m_x m'_y / m'_x m_y < 0$).

JA9618715